Simone Raoux • Matthias Wuttig
Editors

Phase Change Materials

Science and Applications

Editors
Simone Raoux
IBM Almaden Research Center
650 Harry Road
San Jose, CA 95120
USA

Matthias Wuttig
1. Physikalisches Institut (1A)
RWTH Aachen University
52056 Aachen
Germany

ISBN 978-0-387-84873-0 e-ISBN 978-0-387-84874-7
DOI 10.1007/978-0-387-84874-7

Library of Congress Control Number: 2008935619

© Springer Science+Business Media, LLC 2009
All rights reserved. This work may not be translated or copied in whole or in part without the written permission of the publisher (Springer Science+Business Media, LLC, 233 Spring Street, New York, NY 10013, USA), except for brief excerpts in connection with reviews or scholarly analysis. Use in connection with any form of information storage and retrieval, electronic adaptation, computer software, or by similar or dissimilar methodology now known or hereafter developed is forbidden.
The use in this publication of trade names, trademarks, service marks, and similar terms, even if they are not identified as such, is not to be taken as an expression of opinion as to whether or not they are subject to proprietary rights.

Printed on acid-free paper

springer.com

Contents

1. History of Phase Change Memories 1
Chung H. Lam
1.1 The Discovery of Phase Change Materials 1
1.2 Early Electronic Computers and Memory Systems 2
1.3 Pioneers in Phase Change Memory 4
1.4 Early Attempts with Phase Change Memory 9
1.5 Rebirth of Phase Change Memory 10
References 14

Part I: Material Science: Theory and Experiment

2. Density Functional Theory Calculations for Phase Change Materials 17
Wojciech Wełnic
2.1 Introduction 17
2.2 The Theorem of Hohenberg and Kohn 18
2.3 The Kohn-Sham Equation 20
2.4 The Local Density Approximation 22
2.5 Beyond Density Functional Theory 23
2.6 Application of DFT in the Field of Phase Change Materials 24
2.6.1 Structure Determination 25
2.6.2 Electronic Properties 29
References 36

3. Nature of Glasses 39
Punit Boolchand, Matthieu Micoulaut, and Ping Chen
3.1 Introduction 39
3.2 Thermodynamics of the Glass Transition 41
3.3 Glass Transition from Dynamics 43
3.4 Glass Forming Tendency 44
3.4.1 Compositional Trends of the Glass Transition Temperature 46
3.5 Calorimetric Measurement of the Glass Transition Temperature and Related Thermal Properties 48
3.6 Three Generic Classifications of Glasses and Glass Transitions 51

3.7 Elastic Phases in Ionic and Super-ionic Glasses 54
3.8 Ideal Glasses and Self-organization of Networks 54
3.9 Does the View Below the Glass Transition Temperature Correlate with the View above the Glass Transition Temperature? 56
3.10 Glass Formation in Hydrogen Bonded Networks 57
3.11 Epilogue 59
References 59

4. Structure of Amorphous Ge-Sb-Te Solids 63
Stephen R. Elliott
4.1 Introduction 63
4.2 Structural Order in Amorphous Materials 64
4.2.1 Short-range Order 64
4.2.2 Medium-range Order 65
4.2.3 Long-range Structure 66
4.3 Experimental Structural Probes 67
4.4 Structural Modeling 68
4.5 The Structure of Amorphous Phase-change Materials 69
4.5.1 Experimental Studies 69
4.5.2 Simulational Studies 72
4.6 Summary 78
References 79

5. Experimental Methods for Material Selection in Phase-change Recording 81
Liesbeth van Pieterson
5.1 Introduction 81
5.2 Reversible Switching 82
5.3 Phase-change Materials 84
5.3.1 Crystallization by Nucleation and Growth 86
5.3.2 Crystallization Dominated by Crystal Growth 88
5.4 Archival Life Stability 89
5.5 Crystallization Rate 91
5.6 Material Optimization 93
5.7 Outlook 97
References 98

6. Scaling Properties of Phase Change Materials 99
Simone Raoux
6.1 Introduction 99
6.2 Thin Films of Phase Change Materials 100
6.2.1 Crystallization Temperature as a Function of Film Thickness ... 101
6.2.2 Crystallization Rate as a Function of Film Thickness 105

6.2.3 Change in Optical Constants and Electrical and Thermal Parameters as a Function of Film Thickness 108
6.2.4 Limits of Storage Density in Thin Films 109
6.3 Phase Change Nanowires 111
6.4 Phase Change Nanoparticles 114
6.5 Scaling in Time – Switching Speed of Phase Change Materials 118
References. 120

7. Crystallization Kinetics 125
Johannes A. Kalb
7.1 Theory 125
7.1.1 Homogeneous Crystal Nucleation 125
7.1.2 Heterogeneous Crystal Nucleation 133
7.1.3 Crystal Growth 135
7.2 Measurements 138
7.2.1 Crystallization Parameters Around the Glass Transition Temperature 138
7.2.2 Crystallization Parameters Close to the Melting Temperature 142
References 145

8. Short and Long-Range Order in Phase Change Materials 149
Paul Fons
8.1 Historical Background 149
8.1.1 Glass Formation Process 150
8.2 Long-Range Order 151
8.2.1 GeTe 152
8.2.2 Ge-Sb-Te Alloys 154
8.3 Short-Range Order 160
8.3.1 X-ray Absorption 160
8.3.2 Short Range Order in Sb-Te Alloys 170
References 171

9. Optical and Electrical Properties of Phase Change Materials 175
Bong-Sub Lee and Stephen G. Bishop
9.1 Introduction 175
9.2 Optical Constants and Optical Bandgap 176
9.2.1 Determination of the Optical Constants and Absorption Coefficient 176
9.2.2 Optical Bandgap 179
9.2.3 Infrared Absorption: Band Tails and Free Carrier Absorption 181
9.2.4 Effects of Composition and Preparation Conditions 182

9.3 Photo-induced Effects ... 184
9.3.1 Photo-induced Current and Optical Nonlinearity ... 184
9.3.2 Photo-Oxidation ... 185
9.4 Conductivity and Phase Transformation ... 186
9.4.1 Temperature-dependence of Resistivity ... 186
9.4.2 Intermediate States: Percolation and Multilevel Recording ... 187
9.4.3 Effects of Composition and Processing Conditions ... 188
9.5 Electronic Transport Properties and Band Structure ... 189
9.5.1 Characterization of Transport Properties ... 189
9.5.2 Hexagonal $Ge_2Sb_2Te_5$ ... 191
9.5.3 Face-centered-cubic $Ge_2Sb_2Te_5$ ... 193
9.5.4 Amorphous $Ge_2Sb_2Te_5$ ... 194
9.6 Perspective for the Future ... 194
References ... 195

10. Development of Materials for Third Generation Optical Storage Media ... 199
Noboru Yamada
10.1 Introduction ... 199
10.2 Requirements for a Phase-change Material ... 200
10.3 Why Chalcogenide Semiconductors for Optical Memory? ... 202
10.4 Merits and Demerits of the Te Based Eutectic Alloys ... 203
10.5 Merits and Demerits of the Te-based Single Phase Materials ... 206
10.6 From Eutectic to Single Phase Compositions ... 208
10.7 Discovery of the GeTe-Sb_2Te_3 Pseudo-binary System ... 209
10.8 Importance of the Cubic Structure and Vacancies ... 213
10.9 Secrets of the Present Phase-change Materials I ... 215
10.10 Materials for Blue Laser and Multi-layer Applications ... 219
10.11 Secrets of Present Phase-change Materials II ... 222
10.12 Conclusions ... 223
References ... 224

11. Novel Deposition Methods ... 227
Delia J. Milliron, Qiang Huang and Yu Zhu
11.1 Chemical Vapor Phase Deposition ... 227
11.2 Electrodeposition ... 233
11.3 Solution-phase Deposition ... 238
11.4 Nanomaterials ... 241
11.5 Conclusions ... 243
References ... 244

Part II: Applications: Optical, Solid State Memory and Reconfigurable Logic

12. Optical Memory: From 1st to 3rd Generation and its Future 251
Luping Shi
12.1 Introduction 251
12.2 Three Generations of Optical Media 252
12.2.1 The First Generation: Compact Discs (CDs) 253
12.2.2 The Second Generation: Digital Versatile Disks (DVDs) 253
12.2.3 The Third Generation: Blu-ray Discs (BDs)........................... 256
12.3 The Basic Principle of Optical Recording 257
12.4 Phase-change Optical Recording and Related Technologies.............. 260
12.4.1 Phase-Change Optical Storage.. 260
12.4.2 Techniques for Phase-Change Optical Storage....................... 270
12.5 The Future of Optical Storage 279
References 282

13. 4th Generation Optical Memories Based on Super-resolution Near-field structure (Super-RENS) and Near-field Optics 285
Junji Tominaga
13.1 Introduction 285
13.2 Diffraction Limit and Near-Field Optics 286
13.3 Small Aperture and Non-propagating Photons 288
13.4 Super-resolution Near-field Structure (Super-RENS) Principle to Retrieve Non-propagating Light 290
13.5 Origin of the Strong Scattered Signals for 4th Generation Super-RENS Disks 292
13.6 Beyond Super-RENS.. 296
References 297

14. Phase Change Memory Device Modeling 299
Daniele Ielmini
14.1 Introduction 299
14.2 Device Operation.. 300
14.3 Modeling of Electrical Conduction in the Amorphous Phase............. 302
14.4 Threshold Switching in the Amorphous Chalcogenide 306
14.5 Modeling the Electrical Conduction in the Crystalline Chalcogenide 308
14.6 Electro-thermal Modeling of the Programming Characteristics 309
14.7 Modeling the Amorphous to Crystalline Phase Transformation 314
14.8 Modeling the Structural Relaxation in the Amorphous Phase............ 320
14.9 Summary and Outlook.. 325
References 327

15. Phase Change Random Access Memory Advanced Prototype Devices and Scaling 331
Yi-Chou Chen
15.1 Introduction 331
15.2 Device Scaling by Reducing the Electrode Contact Area 332
15.2.1 The Heater Structure 333
15.2.2 The Edge Contact Structure 337
15.2.3 μTrench Structure 338
15.2.4 The Ring Structure 338
15.3 Device Scaling by Reducing the Phase Change Material Volume 339
15.3.1 The Pillar Structure 340
15.3.2 The Line Structure 341
15.3.3 The Bridge Structure 342
15.4 Other Prototype Devices 343
15.4.1 Scaling Both the Material and the Contact 344
15.4.2 Multi-level Cell 345
15.4.3 Confined Structure 345
15.5 Advanced Device Testing 347
15.6 Summary 349
References 350

16. Phase Change Memory Cell Concepts and Designs 355
Roberto Bez, Robert J. Gleixner, Fabio Pellizzer, Agostino Pirovano and Greg Atwood
16.1 Introduction 355
16.2 Technology Overview 356
16.3 Phase Change Memory Cell Electrical Characterization 361
16.4 Phase Change Memory Cell Reliability 368
16.4.1 Data Retention Characterization 369
16.4.2 Retention Behavior with Device Scaling 376
16.4.3 Cycling Endurance 377
16.5 Summary and Outlook 378
References 379

17. Phase Change Random Access Memory Integration 381
Matthew J. Breitwisch
17.1 Introduction 381
17.2 Phase Change Random Access Memory Design Basics 382
17.3 Review of Desired Phase Change Memory Cell Characteristics 386
17.4 The Access Device 390
17.5 Device Design Considerations 393
17.5.1 The Mushroom Cell without or with Bottom Ring Electrode 393
17.5.2 The Pillar Cell 397

17.5.3 The μTrench Cell 399
17.5.4 The Pore Cell 399
17.6 Multi-Level Phase Change Random Access Memory 403
17.7 Concluding Remarks 406
References 406

18. Reconfigurable Logic 409
James Lyke
18.1 Introduction 409
18.2 Digital System Basics 410
18.3 Simple Configurable Digital Systems 414
18.4 Considerations in Computation Architectures 419
18.5 Multi-valued Systems 420
18.6 Threshold Logic 422
18.7 Artificial Neural Networks 425
18.8 Other Analog-domain Programmable Systems 426
18.9 Conclusions 429
References 429

Author Bios 431

Index 437

Part I:
Material Science: Theory and Experiment

7. Crystallization Kinetics

Johannes A. Kalb

Abstract The classical theory of steady state crystal nucleation is discussed, as originally developed by Gibbs, Volmer, Weber, Becker, Döring, Turnbull and Fisher. A particular focus is drawn on the implications of heterogeneous nucleation sites, which can increase the homogeneous nucleation rate by many orders of magnitude. Classical theory of crystal growth is covered as well.

In Sect. 7.2, these theories are applied to measurements of nucleation and growth parameters in amorphous and liquid phase change materials by calorimetry and microscopy. The results contribute to a better understanding of the kinetics of the phase transformation in these materials, which helps to develop next-generation phase change media and to scale them to smaller dimensions.

7.1 Theory

Two processes are involved in the crystallization of a liquid or an amorphous solid (hereafter: parent phase):

1. First, crystallization is initiated by crystal nucleation. In the simplest case, this occurs in the interior of the parent phase, i. e., without the involvement of a "foreign" substance. This is called *homogeneous nucleation* (Sect. 7.1.1). If the parent phase is in contact with a foreign substance that acts as a preferred nucleation site (like an impurity or a container wall), nucleation is called *heterogeneous* (Sect. 7.1.2).
2. Subsequently, a stable crystal cluster grows to macroscopic size (crystal growth, Sect. 7.1.3).

7.1.1 Homogeneous Crystal Nucleation

The basic concept for nucleation theory was provided by Gibbs in 1878 (Sect. 7.1.1.1, [7.1-7.3]). This early treatment is still purely thermodynamic and describes cluster formation of a new phase inside the parent phase. Using this approach, the first *kinetic* model for nucleation was proposed by Volmer and Weber in 1926 (Sect. 7.1.1.2, [7.2-7.4]) and has served as a basis for a further improve-

S. Raoux, M. Wuttig (eds.), *Phase Change Materials*,
DOI 10.1007/978-0-387-84874-7_7, © Springer Science+Business Media, LLC 2009

ment by Becker and Döring in 1935 (Sect. 7.1.1.3, [7.2, 7.3, 7.5]). Finally, in 1949, Turnbull and Fisher obtained an expression for the pre-exponential factor of the nucleation rate in a condensed phase (Sect. 7.1.1.4, [7.2, 7.3, 7.6]). Today, the theory is collectively known as the *classical nucleation theory* by Volmer, Weber, Becker, Döring, Turnbull and Fisher.

7.1.1.1 Thermodynamics of Cluster Formation (Gibbs, 1878)

In the parent phase, atoms approach each other statistically, forming crystalline clusters by thermodynamic fluctuations. For simplicity, these clusters are assumed spherical with radius r. The equilibrium cluster distribution is then given by Boltzmann statistics [7.7],

$$N^{equ}(r) = N_0 \cdot \exp\left(-\frac{\Delta G_{cluster}(r)}{k_B T} \right), \tag{7.1}$$

where $\Delta G_{cluster}$ (r) is the reversible work for crystal cluster formation, k_B the Boltzmann constant, T the absolute temperature, N_0 the total number of atoms in the liquid and $N^{equ}(r)$ the number of clusters of radius r at equilibrium (N_0 and $N^{equ}(r)$ are normalized per unit volume). $\Delta G_{cluster}$ (r) can be expressed as a sum of two contributions [7.1-7.3]:

$$\Delta G_{cluster}(r) = -\Delta G_{lc,V} \cdot \frac{4}{3}\pi r^3 + \sigma \cdot 4\pi r^2 . \tag{7.2}$$

$\Delta G_{lc,V}(T)$ is the (Gibbs) free energy difference between the parent and the crystalline phase per unit volume. It is zero at the melting temperature T_m and defined to be positive below T_m. $\Delta G_{lc,V}(T)$ increases with increasing undercooling below T_m, i. e., it increases with decreasing temperature T.[1] The second term in Eq. (7.2) results from the creation of an interface between the cluster and the liquid. This term is positive and therefore energetically not favorable. The quantity $\sigma > 0$ is the interfacial free energy (hereafter: interfacial free energy). An additional elastic strain energy term due to the density change upon crystallization can be neglected in Eq. (7.2) unless the parent phase is very viscous [7.2].

Figure 7.1 qualitatively displays the evolution of $\Delta G_{cluster}$ (r). The curve passes through a maximum, which can be obtained by solving $\frac{\partial \Delta G_{cluster}(r)}{\partial r} = 0$. The

[1] Note that a complete description for alloys would employ the liquidus temperature T_l instead of the melting temperature T_m, which would go beyond the scope of this chapter [7.8].

maximum occurs because the surface-to-volume ratio is large for small clusters. The position of the maximum is (Fig. 7.1)

$$r_c = \frac{2\sigma}{\Delta G_{lc,V}}, \tag{7.3}$$

and the height is

$$\Delta G_c := \Delta G_{cluster}(r_c) = \frac{16\pi}{3} \frac{\sigma^3}{\left(\Delta G_{lc,V}\right)^2}. \tag{7. 4}$$

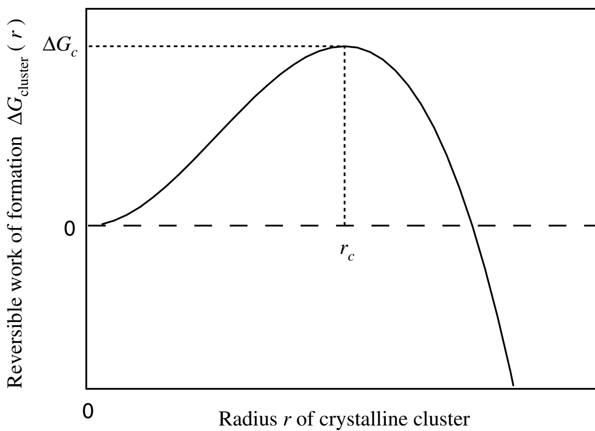

Fig. 7.1. Reversible work $\Delta G_{cluster}$ (r) for the formation of crystalline clusters of radius r in the parent phase ($T < T_m$). Clusters decay for $r < r_c$ and grow for $r > r_c$.

The quantity r_c is called the *critical radius*, which is on the order of nanometers [7.2, 7.3]. A cluster of radius r_c is called a *critical cluster* and ΔG_c (T) the *critical work for cluster formation*. $\Delta G_{cluster}$ (r) increases for $r < r_c$. Hence, clusters of size $r < r_c$ are energetically not favorable and spontaneously decay. However, for $r > r_c$, clusters grow due to a gain in free energy. Therefore, ΔG_c can be considered an activation barrier against crystallization. The existence of this barrier enables undercooling of a liquid below T_m without immediate crystallization. Simply speaking, nucleation in this early Gibbs treatment is the formation of post-critical clusters of size $r > r_c$.

7.1.1.2 Model Based on Equilibrium Distribution of Clusters (Volmer and Weber, 1926)

Volmer and Weber developed the first *kinetic* model for nucleation. Their model utilizes the equilibrium cluster distribution [Eq. (7.1)]. However, since $N^{equ}(r)$

becomes unphysical for $r > r_c$ (cluster number increases with increasing radius r, dashed in Fig. 7.2), it was ignored and set to zero: $N^{equ}(r > r_c) = 0$ [7.2, 7.3].

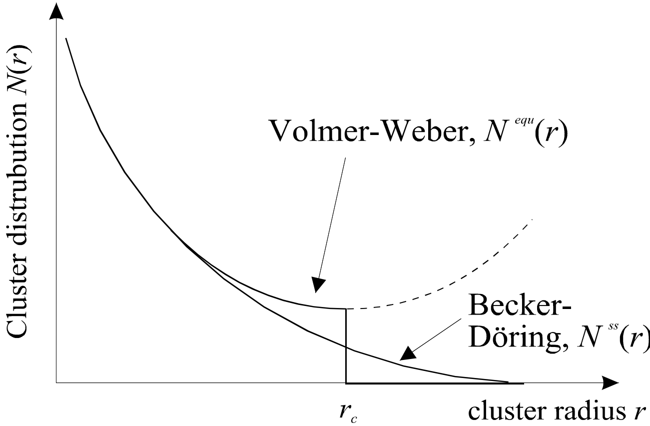

Fig. 7.2. Statistical cluster distribution function. $N^{equ}(r)$: Volmer-Weber model [equilibrium, Eqs. (7.1) and (7.2)]. $N^{ss}(r)$: Becker-Döring model (steady state). r_c is the radius of the critical cluster. $N^{ss}(r_c)=1/2 \cdot N^{equ}(r_c)$. The dashed part of the curve was ignored by Volmer and Weber: $N^{equ}(r > r_c) = 0$.

For $r = r_c$,

$$N^{equ}(r_c) = N_0 \cdot \exp\left(-\frac{\Delta G_c}{k_B T}\right). \tag{7.5}$$

Volmer and Weber assumed that nucleation occurs when a critical cluster acquires one more atom. The nucleation rate I^{equ} (dimension: $1/\mathrm{m}^3\mathrm{s}$) is then given by [7.2, 7.3]

$$I^{equ} = s_c \cdot k \cdot N^{equ}(r_c) = s_c \cdot k \cdot N_0 \cdot \exp\left(-\frac{\Delta G_c}{k_B T}\right), \tag{7.6}$$

where k is the arrival rate of parent phase atoms to the critical crystalline cluster (number of arrivals per atom on the cluster surface per unit time, dimension: 1/s). s_c is the number of surface atoms in the critical cluster.

7.1.1.3 Steady State Model (Becker and Döring, 1935)

The Volmer-Weber model assumes that a critical cluster grows to macroscopic size as soon as it becomes post-critical by the addition of one more parent phase atom. Its main deficiency is that it neglects that post-critical clusters ($r > r_c$) can still decay with a certain probability (though they are more likely to grow), and

that critical clusters ($r = r_c$) grow or shrink with equal probability (since $\partial \Delta G_{cluster}(r) / \partial r|_{r=r_c} = 0$). Becker and Döring have argued that the true cluster distribution $N^{ss}(r)$ in steady state (Fig. 7.2) does not abruptly fall to zero at $r = r_c$, but takes a value of $N^{ss}(r_c) = 1/2\ N^{equ}\ (r_c)$ and decreases gradually to zero for large cluster sizes [7.2, 7.3, 7.5]. For small cluster sizes, N^{ss} approaches N^{equ}.

After a few additional assumptions, Becker and Döring obtain the following expression for the steady state nucleation rate I^{ss} [7.2, 7.3]:

$$I^{ss} = s_c \cdot k \cdot N_0 \cdot \underbrace{\frac{1}{i_c} \cdot \left(\frac{\Delta G_c}{3\pi k_B T} \right)^{\frac{1}{2}}}_{\Gamma_z} \cdot \exp\left(-\frac{\Delta G_c}{k_B T} \right), \tag{7.7}$$

where i_c is the number of atoms in the critical cluster. Equation (7. 7) differs from the Volmer-Weber equation [Eq. (7.6)] only by the Zeldovich factor Γ_z, which only has a weak temperature dependence. Based on analytical and numerical studies, Γ_z is between 1/100 and 1/10 in most cases [7.2, 7.3, 7.9].

As the nucleation rate is far more sensitive to slight changes in ΔG_c than to the exact value of the pre-exponential factor [7.2], the Becker-Döring expression [Eq. (7.7)] is essentially identical to the Volmer-Weber expression [Eq. (7.6)] for all practical purposes. However, the importance of the Becker-Döring theory is that the kinetic problem has been treated correctly [7.2].

7.1.1.4 The Kinetic Pre-factor of the Nucleation Rate (Turnbull and Fisher, 1949)

Volmer, Weber, Becker and Döring originally developed their theories for the case of a *gaseous* parent phase (i. e., vapor condensation). For this case, the arrival rate k [Eq. (7.7)] is readily obtained by the theory of gases (not discussed here, [7.2]). However, Turnbull and Fisher were the first to evaluate the pre-exponential factor in Eq. (7.7) for crystal nucleation in an undercooled liquid or an amorphous phase [7.2, 7.3, 7.6]. They differentiated between two limiting cases: diffusion-limited and collision-limited crystallization kinetics. In both cases, the composition of the liquid and the crystalline cluster are the same. "Diffusion-limited" therefore refers to the nature of a *local* rearrangement (diffusive jump of an atom across the liquid-crystalline interface), *not* to the presence of a long-range diffusion field.

1. For diffusion-limited crystallization, changes of neighbors and/or coordination number are necessary for crystallization. This usually applies to metallic alloys, ionic materials, covalent materials and is also observed for phase change materials as discussed in more detail in Sect. 7.2. The frequency of diffusive

jumps k [Eq. (7.7)] across the interface per interface atom is according to Turnbull and Fisher

$$k = \frac{6D}{\lambda^2} \qquad \text{(diffusion-limited)} \qquad (7.8)$$

where D is associated with the diffusivity in the liquid or amorphous phase (not in the crystal). The parameter $\lambda = \Omega^{1/3}$ is the average interatomic distance (Ω = atomic volume).

2. For collision-limited crystallization, atomic neighbors generally do not have to change by diffusive rearrangements upon crystallization. Instead, atomic movement from the liquid to the crystalline cluster can be accomplished by thermal vibration. Hence, crystallization is governed by the collision of the atoms. This usually occurs only in pure metals and in van der Waals bonded materials but not in phase change materials as discussed in more detail in Sect. 7.2. The arrival rate constant k [Eq. (7.7)] is then equal to the collision rate at which the atoms attempt to join the crystalline cluster:

$$k = \frac{u_{\text{sound}}}{\lambda} \qquad \text{(collision-limited).} \qquad (7.9)$$

u_{sound} is the sound velocity in the liquid or amorphous phase, which is characteristic for the vibrational motion of the atoms.

Substituting Eq. (7.8) into Eq. (7.7) gives the nucleation rate for diffusion-limited crystallization:

$$I^{ss} = s_c \cdot \frac{6D}{\lambda^2} \cdot N_0 \cdot \Gamma_z \cdot \exp\left(-\frac{\Delta G_c}{k_B T}\right) \qquad \text{(diffusion-limited).} \qquad (7.10)$$

Approximating the diffusivity D locally with an Arrhenius equation, $D \propto \exp\left[-E_D / \left(k_B T\right)\right]$, where $E_D = -\partial \ln D / \partial\left[1/\left(k_B T\right)\right]$ is the (local) activation energy of the diffusivity and k_B the Boltzmann constant, gives the (local) activation energy $E_{I^{ss}}$ of the steady-state nucleation rate I^{ss}:

$$E_{I^{ss}} = E_D + \Delta G_c \qquad \text{(diffusion-limited).} \qquad (7.11)$$

It is often helpful to express I^{ss} in terms of the liquid shear viscosity η, which is easier to obtain experimentally than the liquid diffusivity D. Using the Stokes-Einstein equation,

$$\eta D = \frac{k_B T}{3\pi\lambda}, \tag{7.12}$$

which relates D and η, gives

$$I^{ss} = s_c \cdot \frac{2k_B T}{\eta\pi\lambda^3} \cdot N_0 \cdot \Gamma_z \cdot \exp\left(-\frac{\Delta G_c}{k_B T}\right) \quad \text{(diffusion-limited).} \tag{7.13}$$

Note that Eq. (7.12) implies that the (local) activation energies of diffusivity E_D and viscosity E_η are equal if the viscosity is approximated (locally) by an Arrhenius equation, $\eta \propto \exp\,[E_\eta / (k_B T)]$:

$$E_D = E_\eta. \tag{7.14}$$

The linear term in T on the right side of Eq. (7.12) varies slowly with T compared to the exponential terms on the left side and therefore does not contribute to Eq. (7.14). The Stokes-Einstein equation has been found to hold for a large variety of undercooled liquids. Violations of this relation have been reported only for some fragile liquids [7.10-7.13]. Substituting $N_0 = 1/\lambda^3 = 1/\Omega$ and estimating the pre-exponential factor by $N_0 \sim 10^{28}$ m^{-3}, $s_c \sim 10$, $T \sim 1000$ K, and $\Gamma_z \sim 1/100$ [7.2], this gives

$$I^{ss} = \frac{10^{36}}{\eta} \exp\left(-\frac{\Delta G_c}{k_B T}\right) \frac{1}{\text{m}^3\text{s}} \quad \text{(diffusion-limited),} \tag{7.15}$$

where η is the numerical value of the liquid shear viscosity in units of poise.[2]

Substituting Eq. (7.9) into Eq. (7.7) gives the nucleation rate for collision-limited crystallization,

$$I^{ss} = 10^{39} \exp\left(-\frac{\Delta G_c}{k_B T}\right) \frac{1}{\text{m}^3\text{s}} \quad \text{(collision-limited),} \tag{7.16}$$

where $\lambda \sim 3$ Å and $u_{\text{sound}} \sim 1000$ ms^{-1} have been used as a typical example [7.2].

The uncertainty of the pre-exponential factors in Eqs. (7.15) and (7.16) is about two to four orders of magnitude [7.2]. However, as the exponential term varies so rapidly with ΔG_c upon undercooling, the value of ΔG_c that is required to give a fixed nucleation rate at a specific temperature is insensitive to the exact

[2] 1 Pa s =10 poise.

value of the pre-exponential factor [7.2, 7.3]. This applies even more to the interfacial energy σ, since it is raised to the third power in the exponential.

Equations (7.15) and (7.16) coincide for practical purposes at low undercooling (i. e., at a temperature slightly below T_m), where the viscosity is roughly independent of temperature (Fig. 7.3) and usually on the order of 10^{-1} - 10^{-3} poise. Both equations have been used widely and successfully to model experimental data on crystal nucleation in undercooled liquids [7.2, 7.8, 7.14-7.18].

The nucleation rate I^{ss} for diffusion-limited crystallization [Eq. (7.15)] becomes negligibly small close to the melting point T_m, where ΔG_c (T_m) = ∞ [since $\Delta G_{lc,V}$ (T_m) = 0, Eq. (7.4)], and close to the glass transition temperature T_g, where the viscosity strongly increases upon cooling from the liquid (Fig. 7.3).

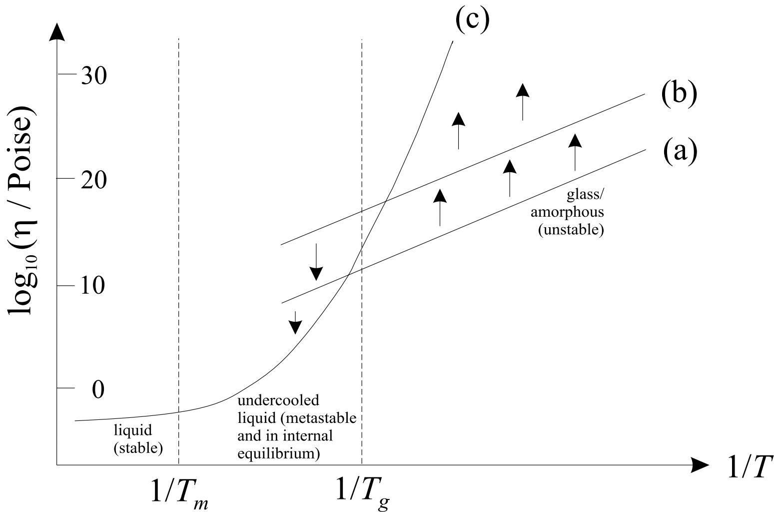

Fig. 7.3. Viscosity η in various stability regimes (T_g: glass transition temperature, which marks the boundary between a glass (amorphous phase) and an undercooled liquid; T_m: melting temperature). Stable equilibrium for $T > T_m$, metastable equilibrium (undercooled liquid) for $T_g < T < T_m$ and amorphous (frozen isoconfigurational states, non-equilibrium) for $T < T_g$. The amorphous states are unstable with respect to structural relaxation, i. e., they alter their structure towards the equilibrium structure of the undercooled liquid, which is indicated by the arrows. The slower the cooling rate, the longer the metastable equilibrium can be maintained upon cooling: (a) Fast cooling. (b) Slow cooling. (c) Hypothetically infinitively slow cooling, which maintains metastable equilibrium at all temperatures [7.19-7.21]. Therefore, T_g depends on the timescale of the experiment, but it usually occurs at a temperature at which the viscosity adopts a value on the order of 10^{12} Pa s = 10^{13} poise [7.22].

Therefore, I^{ss} exhibits a pronounced maximum at a temperature between T_g and T_m. Such a maximum is not present for collision-limited kinetics, where I^{ss} increases continuously upon cooling [Eq. (7.16)], which is not observed for phase change materials (Sect. 7.2).

7.1.2 Heterogeneous Crystal Nucleation

Homogeneous nucleation is an *intrinsic* process. In practice, however, homogeneous nucleation is difficult to identify specifically. Usually, foreign phases like container walls and impurities aid in the nucleation process and thereby increase the nucleation rate. In this case, nucleation is called *heterogeneous*. Heterogeneous nucleation is therefore an *extrinsic* process and can be influenced by the experimental conditions [7.9].

The simplest model for heterogeneous nucleation is due to Volmer [7.23, 7.24]. The model is based on the Gibbs model (Sect. 7.1.1.1) but with a flat substrate, which acts as a heterogeneous nucleation site (Fig. 7.4).

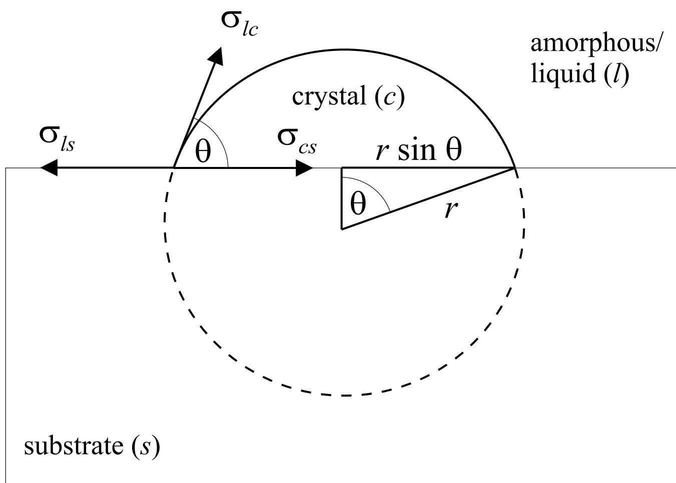

Fig. 7.4. Volmer's spherical cap model for heterogeneous cluster formation. The exposed crystal cluster has the shape of a spherical cap, whose volume is $f(\theta) \cdot 4/3\pi r^3$. The quantities σ_{cs}, σ_{ls} and σ_{lc} are the interfacial energies between the three substances involved. The dashed circle segment is a guide for the eye.

Under the assumption that the phases are isotropic, the interface between the crystalline cluster and the liquid (or amorphous) parent phase must have the same curvature everywhere. Hence, the crystalline cluster grows on the flat substrate like a spherical cap of radius r (Fig. 7.4). As a function of the wetting angle θ (Fig. 7.4), the exposed volume fraction $0 \le f(\theta) \le 1$ relative to a sphere of the same radius r is [7.24]

$$f(\theta) = \frac{(2+\cos\theta)\,(1-\cos\theta)^2}{4}. \tag{7.17}$$

Based on Gibbs' approach [Eq. (7.2)], Volmer [7.23, 7.24] could show that heterogeneous nucleation is preferred over homogeneous nucleation if

$$\sigma_{cs} - \sigma_{ls} < \sigma_{lc}, \tag{7.18}$$

where σ_{cs}, σ_{ls} and σ_{lc} denote, respectively, the crystal-substrate, liquid-substrate and liquid-crystal interfacial energies (Fig. 7.4). In this case, the reversible work for cluster formation *per atom*, $\Delta G_{\text{cluster}}$ (Fig. 7.1), is lower than if the circular cluster surface $\pi\,(r \sin\theta)^2$ were exposed to the liquid. The critical work for heterogeneous cluster formation is then reduced to

$$\Delta G_c^{\text{het}} = \underbrace{\frac{16\pi}{3}\frac{\sigma^3}{\left(\Delta G_{lc,V}\right)^2}}_{\Delta G_c \equiv \Delta G_c^{\text{hom}}} \cdot f(\theta), \tag{7.19}$$

whereas the critical radius remains unchanged[3]: $r_c^{\text{het}} = r_c^{\text{hom}}$. If there is no wetting (homogeneous nucleation, $\theta = 180°$, $f = 1$), Eq. (7.19) reduces to Eq. (7.4), i. e., the substrate does not aid in the nucleation process.

The classical theory for homogeneous nucleation (Sect. 7.1.1) can equally be applied to the case of heterogeneous nucleation [7.2, 7.9]. The only difference is the lower work for critical cluster formation [Eq. (7.19)] and the reduced number of parent phase atoms that can act as a nucleation site: While any parent phase atom can act as a nucleation site for homogeneous nucleation, only those atoms in contact with the impurity can act as a nucleation site for heterogeneous nucleation [7.2, 7.9, 7.25]. If ε is the fraction of parent phase atoms in contact with the heterogeneity (usually $\varepsilon \ll 1$), then the steady state nucleation rate for heterogeneous nucleation and diffusion-limited kinetics, $I^{ss,\text{het}}$, is

$$I^{ss,\text{het}} = \varepsilon \cdot s_c \cdot \frac{6D}{\lambda^2} \cdot N_0 \cdot \Gamma_z \cdot \exp\left(-\frac{\Delta G_c^{\text{het}}}{k_B T}\right) \frac{1}{\text{m}^3\text{s}} \tag{7.20}$$

[cf. Eq. (7.10)] with a (local) activation energy of

$$E_{I^{ss},\text{het}} = E_D + \Delta G_c^{\text{het}}. \tag{7.21}$$

Since $\Delta G_c^{\text{het}} < \Delta G_c$ for $f(\theta) < 1$ [Eq. (7.19)] it follows that $E_{I^{ss},\text{het}} < E_{I^{ss}}$ [Eq. (7.11)]. The ratio of heterogeneous to homogenous nucleation rate (dimensionless) at a given temperature is then

---

[3] However, note that the *number of atoms* in the critical cluster is reduced by the factor $f(\theta)$ for heterogeneous nucleation compared to homogeneous nucleation for the same critical radius r_c (Fig. 7.4).

$$\frac{I^{ss,\text{het}}}{I^{ss,\text{hom}}} = \varepsilon \cdot \exp\left(\frac{\Delta G_c}{k_B T} \cdot \left[1 - f(\theta) \right] \right), \tag{7.22}$$

where $I^{ss,\text{hom}} \equiv I^{ss}$. Equation (7.22) applies to both diffusion-limited and collision-limited crystallization. Figure 7.5 shows a plot of Eq. (7.22) for a reasonable parameter of $\varepsilon = 10^{-6}$ [7.9] for three values of the critical work for *homo*geneous cluster formation, ΔG_c.

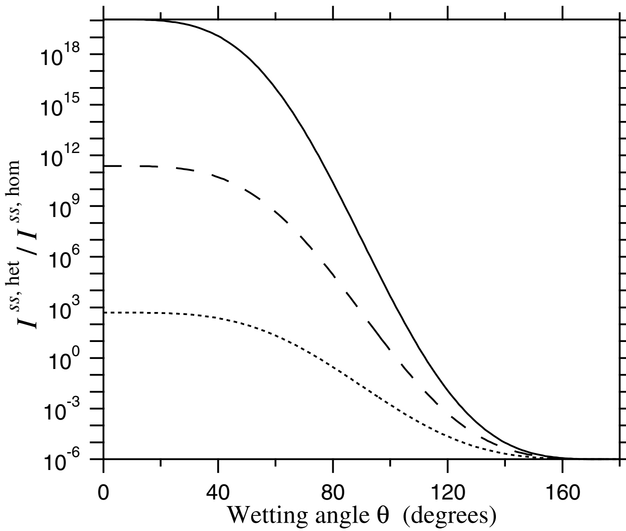

Fig. 7.5. Ratio of heterogeneous to homogenous nucleation rate $I^{ss,\text{het}} / I^{ss,\text{hom}}$ (dimensionless) at constant temperature, calculated from Eqs. (7.22) and (7.17) for $\varepsilon = 10^{-6}$.
Solid line: $\Delta G_c = 60\ k_B T$.
Dashed line: $\Delta G_c = 40\ k_B T$.
Dotted line: $\Delta G_c = 20\ k_B T$.

This illustrates the drastic influence of heterogeneities on the nucleation rate by many orders of magnitude. Usually, heterogeneous nucleation rates are observed to be far higher than homogeneous nucleation rates [7.2, 7.3], which implies that θ must be small (Fig. 7.5). In any case, since heterogeneous nucleation occurs *in addition* to homogeneous nucleation, $I^{ss,\text{total}} = I^{ss,\text{het}} + I^{ss,\text{hom}}$, the nucleation rate is always lowest for purely homogeneous nucleation ($I^{ss,\text{het}} = 0$).

7.1.3 Crystal Growth

The nucleation theory describes the formation of stable crystal clusters. Those can grow to macroscopic size. There are two possibilities: interface-controlled growth (Sect. 7.1.3.1) and growth controlled by a long-range diffusion field (Sect. 7.1.3.2).

7.1.3.1 Interface-controlled Growth

If there is no phase separation upon crystallization, the composition of parent phase and crystal cluster are the same at all times. Therefore, growth is controlled by rearrangement processes *only* at the liquid-crystalline interface and is therefore called *interface-controlled* [7.2]. Such a rearrangement process may either involve a diffusive jump in the case of diffusion-limited kinetics or an atomic collision in the case of collision-limited kinetics (Sec. 7.1.1.4). The rearrangement frequency is in both cases independent of the interface position so that the growth velocity u is time-independent. The crystal growth velocity is then [7.2]

$$u = \gamma_S \cdot \lambda \cdot k \cdot \left[1 - \exp\left(-\frac{\Delta G_{lc,\text{atom}}(T)}{k_B T} \right) \right] \quad (T \leq T_m) \qquad (7.23)$$

where $0 \leq \gamma_s \leq 1$ is the fraction of sites where a new atom can be incorporated. λ is the average interatomic distance (i. e., the distance that the interface moves by each rearrangement), and $\Delta G_{lc,\text{atom}} > 0$ is the (Gibbs) free energy difference between parent phase and crystal *per atom*. The square bracket term in Eq. (7.23) results from thermally activated atomic transfer across the liquid-crystalline interface in *both* directions. The value of the rate constant k is the same as for nucleation [Eqs. (7.8) and (7.9)]. For diffusion-limited kinetics (as observed for phase change materials), this gives [7.2]

$$\begin{aligned} u &= \gamma_S \cdot \frac{6D}{\lambda} \left[1 - \exp\left(-\frac{\Delta G_{lc,\text{atom}}(T)}{k_B T} \right) \right] \\ &= \gamma_S \cdot \frac{2 k_B T}{\eta \pi \lambda^2} \left[1 - \exp\left(-\frac{\Delta G_{lc,\text{atom}}(T)}{k_B T} \right) \right] \quad (T \leq T_m), \end{aligned} \qquad (7.24)$$

where Eq. (7.12) has been used. At the melting temperature T_m, the growth velocity u is zero since $\Delta G_{lc,\text{atom}}(T_m) = 0$. Close to T_g, the square bracket term in Eq. (7.24) varies slowly with temperature compared to the diffusivity D or viscosity η (Fig. 7.3) and can therefore be set as a constant. Therefore:

$$u \propto D \propto \frac{1}{\eta} \qquad (T \approx T_g, \text{ diffusion-limited}), \qquad (7.25)$$

which implies that the (local) activation energies of the crystal growth velocity E_u and the diffusivity E_D are equal:

$$E_u = E_D \qquad (T \approx T_g, \text{ diffusion-limited}). \qquad (7.26)$$

Comparing Eq. (7.26) with Eq. (7.11) or (7.21) gives

$$E_{Jss} - E_u = \Delta G_c \qquad (7.27a)$$

$$E_{Jss,\text{het}} - E_u = \Delta G_c^{\text{het}}, \qquad (7.27b)$$

i. e., the activation energies of nucleation rate and growth velocity differ by the critical work for cluster formation.

Since $u\,(T_m) = 0$ and since u becomes negligibly small close to T_g [Eq. (7.25), Fig. 7.3], it exhibits a maximum between T_g and T_m, which is usually located at higher temperature than the maximum for the nucleation rate [Eqs. (7.10) and (7.20)].

For collision-limited kinetics, u increases continuously upon cooling (not observed for phase change materials) and is limited by the velocity of sound [Eqs. (7.9) and (7.23)]:

$$u = \gamma_S \cdot u_{\text{sound}} \left[1 - \exp\left(-\frac{\Delta G_{lc,\text{atom}}}{k_B T} \right) \right] \qquad (T \le T_m). \qquad (7.28)$$

7.1.3.2 Growth Controlled by Long-range Diffusion

If there is a composition change upon crystallization, *long range* diffusive atomic transport controls the growth velocity because the liquid depletes in certain components close to the liquid-crystalline interface. This depletion becomes more pronounced with increasing time, so that the growth velocity u must decrease with time t. Dimensional analysis of the diffusion equation [7.19, 7.26] gives:

$$u \propto \left(\frac{D}{t} \right)^{\frac{1}{2}}. \qquad (7.29)$$

A time-dependent crystal growth velocity has not been observed in phase change materials that are commonly used for phase change recording (cf. Sect. 7.2). Therefore, this growth mode is not discussed further here.

7.2 Measurements

As discussed in Sect. 7.1, crystallization of an undercooled liquid proceeds on a relatively long timescale just below the melting temperature T_m and close to or below the glass transition temperature T_g. The fastest crystallization is therefore observed at an intermediate temperature T_{int} between T_g and T_m. In optical (or electronic) phase change media, the laser power (or the current) is usually optimized to give high data transfer rates, which implies that crystallization probably occurs somewhere around T_{int}. It is well-established that crystallization in phase change materials near $T = T_{int}$ occurs on timescales of less than 100 ns [7.27-7.31]. Such a short timescale makes it impossible to perform systematic measurements of crystal nucleation rate and crystal growth velocity as a function of temperature around T_{int}. Therefore, crystallization is usually studied either around T_g (Sect. 7.2.1, [7.30-7.42]) or slightly below T_m (Sect. 7.2.2, [7.43]), where crystallization is slow enough to be observed on a laboratory timescale. In some cases, the measured parameters can then carefully be extrapolated to the temperature regime around T_{int}.

7.2.1 Crystallization Parameters Around the Glass Transition Temperature

Frequently, crystallization of amorphous phase change films is studied experimentally around T_g either by Kissinger analysis [7.44], where the crystallization temperature is measured as a function of heating rate [7.32, 7.35, 7.37, 7.38, 7.42], or by Johnson-Mehl-Avrami analysis [7.45, 7.46], where crystallization is monitored isothermally [7.30, 7.35, 7.41]. Both methods determine an *effective* activation energy for crystallization, which includes contributions of both crystal nucleation and crystal growth. Unfortunately, the relative contribution of these two processes remains unknown with these methods. It is therefore more meaningful to measure crystal nucleation rate and crystal growth velocity *independently*, which can only be performed by *direct* observation of crystal size and number as a function of time in an isothermal experiment [7.34, 7.40, 7.41, 7.47, 7.48]. In-situ transmission electron microscopy (TEM) studies have been performed to accomplish this task [7.40], but the drawbacks of this method are imprecise temperature control [7.41] and that the electron beam can influence the crystallization due to additional localized sample heating [7.49]. The experiment described below avoids these difficulties by using ex-situ atomic force microscopy (AFM) in combination with a precise furnace of a power-compensated differential scanning calorimeter (DSC). 30 nm-thin films of composition $Ge_2Sb_2Te_5$, $Ge_4Sb_1Te_5$, $Ge_1Sb_2Te_4$, and $Ag_{0.055}In_{0.065}Sb_{0.59}Te_{0.29}$ (hereafter: AgIn-Sb_2Te) were sputter-deposited on a Si wafer by direct-current magnetron sputtering and annealed isothermally in the DSC around the glass transition temperature T_g. [T_g has been determined in a separate study by DSC to be about 150-200° depending on the alloy (e. g., Fig. 7.6)].

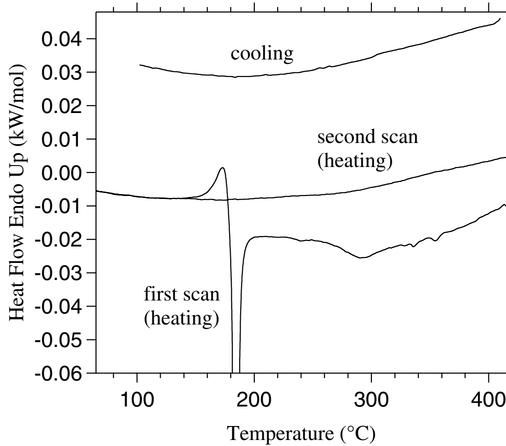

Fig. 7.6. Heat flow as a function of temperature for $Ge_2Sb_2Te_5$ measured by differential scanning calorimetry (DSC). Lowest curve: first scan for the initially fully amorphous sample (heating). The second scan (re-scan of the crystallized sample, heating) is shown for comparison and serves as a baseline for the first scan. Top curve: cooling signal (reproduced in additional scans). The scan rate was ± 40 K/min. The onset of the glass transition temperature T_g, which is usually observed as an endothermic step [7.22], occurs at around 170°. This step cannot be entirely resolved since crystallization interferes (large exothermic peak at around 180-185°, not entirely shown to make the onset of T_g more visible). Details: [7.19, 7.51]. Reprinted from [7.51] with permission of the MRS.

Due to the mass density increase upon crystallization, which induces a reduction in film thickness on the order of 5 % [7.39, 7.50], crystals could be directly observed as depressions in the not-yet-crystallized amorphous film [7.47]. Several AFM scanning and annealing cycles were alternately performed, and the annealing temperature remained the same for the same sample in subsequent anneals (details: [7.19, 7.47, 7.48]). Comparing number density and sizes of crystals on subsequent AFM scans at the same sample location revealed the (heterogeneous) steady-state crystal nucleation rate, $I^{ss,\mathrm{het}}$, and the crystal growth velocity, u. The experiment was repeated at different temperatures to determine their temperature dependencies [7.19, 7.47, 7.48]. Results are displayed in Figs. 7.7 and 7.8. For simplicity, the crystal nucleation rate in Fig. 7. 8 was normalized per unit area (not per unit volume) since cross-sectional TEM has shown that crystals nucleate only heterogeneously at the film surface [7.19, 7.33, 7.48]. Both $I^{ss,\mathrm{het}}$ and u are observed to *increase* with increasing temperature. Hence, as usually expected in alloys, crystallization proceeds diffusion-limited (not collision-limited, Sect. 7.1.1.4 and 7.1.3.1), i. e., Eqs. (7.10), (7.11), (7.20) and (7.21) should apply. For the case of collision-limited kinetics, $I^{ss,\mathrm{het}}$ and u would *decrease* with increasing temperature [Eqs. (7.16) and (7.28)], which is not observed. As a further indication, experience indicates that the crystal growth velocities in Fig. 7.7 are too low to be the result of collision-limited kinetics [7.52].

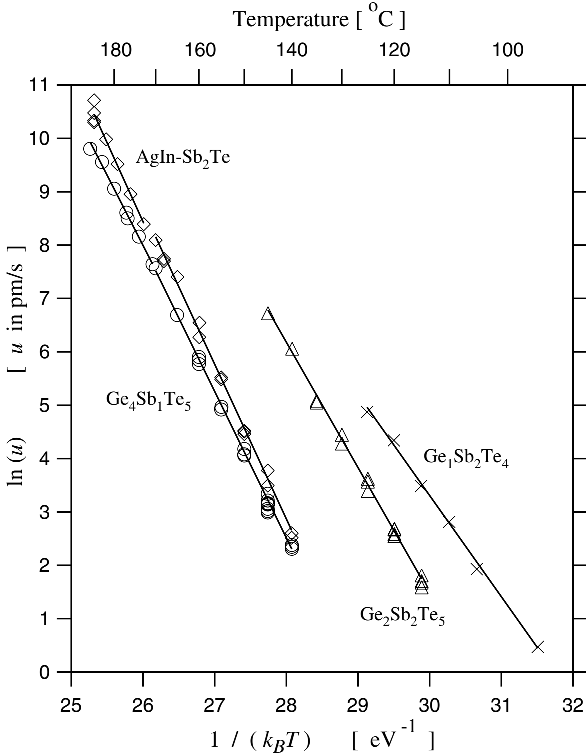

Fig. 7.7. Crystal growth velocity u as a function of temperature T: AgIn-Sb_2Te (squares), $Ge_4Sb_1Te_5$ (circles), $Ge_2Sb_2Te_5$ (triangles) and $Ge_1Sb_2Te_4$ (crosses). The error bars on the velocity are approximately equal to the size of the symbols. The data were fitted with an Arrhenius equation (fit parameters: Table 7.1). For $T > 170°$, a different annealing technique was used, and therefore, the data in this regime were fitted separately (details: [7.19, 7.47]). Reprinted with permission from [7.47]. Copyright [2004], American Institute of Physics.

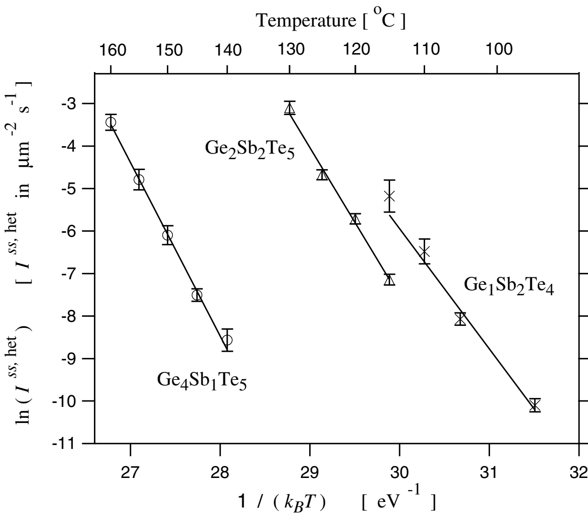

Fig. 7.8. Heterogeneous steady-state crystal nucleation rate $I^{ss,\mathrm{het}}$ as a function of temperature T: $Ge_4Sb_1Te_5$ (circles) $Ge_2Sb_2Te_5$ (triangles) $Ge_1Sb_2Te_4$ (crosses). The data were fitted with an Arrhenius equation (fit parameters: Table 7. 1). Reprinted with permission from [7.48]. Copyright (2005). American Institute of Physics.

Table 7.1. Activation energies E_u and $E_{I^{ss},\mathrm{het}}$ for the crystal growth velocity u and the heterogeneous steady-state nucleation rate $I^{ss,\mathrm{het}}$, respectively. E_u and $I^{ss,\mathrm{het}}$ were obtained from an Arrhenius fit to the data in Figs. 7.7 and 7.8, respectively: $u \propto [- E_u / (k_B T)]$ and $I^{ss} \propto [- E_{I^{ss},\mathrm{het}} / (k_B T)]$. The critical work for heterogeneous cluster formation, $\Delta G_c^{\mathrm{het}}$, was obtained from Eq. (7.27). The activation energy for the isoconfigurational viscosity in the amorphous phase, E_η, was taken from [7.53, 7.54].

Alloy	E_u (eV)	$E_{I^{ss},\mathrm{het}}$ (eV)	$\Delta G_c^{\mathrm{het}}$ (eV)	E_η (eV)
$Ge_4Sb_1Te_5$	2.74 ± 0.03	4.09 ± 0.20	1.35 ± 0.23	1.94 ± 0.09
$Ge_2Sb_2Te_5$	2.35 ± 0.05	3.50 ± 0.17	1.15 ± 0.22	1.76 ± 0.05
$Ge_1Sb_2Te_4$	1.89 ± 0.05	2.82 ± 0.18	0.93 ± 0.23	– [a]
AgIn-Sb_2Te	2.90 ± 0.05	n/a [b]	n/a [b]	1.33 ± 0.09

[a] No data available.

[b] Steady-state nucleation not observed for this alloy.

A time dependence of the crystal growth velocity u could not be observed within error between subsequent anneals of the same sample at the same temperature (Fig. 7.7). This implies that crystal growth occurs interface-controlled (as opposed to growth controlled by long-range diffusion, Sect. 7.1.3), i. e., Eqs. (7.24) – (7.27) should apply [as opposed to Eq. (7.29)].

In the initial stage of crystallization (at short times, i. e., during the first annealing cycle), the crystal nucleation rate for all GeSbTe alloys increased with time due to transient effects (not shown in Fig. 7.8, details: [7.19, 7.48]). This effect occurs since the steady-state cluster distribution N^{ss} (Fig. 7.2) has not yet been developed in the initial stage of crystallization [7.2, 7.24]. After the so-called *incubation time*, the cluster distribution adopts a steady-state value, and therefore, the crystal nucleation rate is time-independent as shown in Fig. 7.8 [cf. Eq. (7.20)]. For AgIn-Sb_2Te, no data are shown in Fig. 7.8 since a steady state could not be observed. Apart from that, the nucleation rate for AgIn-Sb_2Te was far lower than for the GeSbTe alloys (details: [7.19, 7.47, 7.48]). AgIn-Sb_2Te is known to exhibit growth-dominated crystallization upon laser heating, i. e., an amorphous mark in a crystalline matrix re-crystallizes by the growth from the rim of the amorphous mark [7.28, 7.55]. This is in contrast to the GeSbTe alloys, which recrystallize nucleation-dominated, i. e., an amorphous mark re-crystallizes upon laser heating predominantly by nucleation inside the amorphous mark [7.27]. This suggests that the different recrystallization mechanisms observed upon laser heating can be ascribed to the significant qualitative difference in crystal nucleation behavior rather than to the smaller difference in crystal growth velocity (qualitatively similar behavior for all alloys).

The activation energy for the heterogeneous steady state nucleation rate, $E_{I^{ss},\mathrm{het}}$, and for the growth velocity, E_u, is determined from the slope of each

straight line in Figs. 7.7 and 7.8 and given in Table 7. 1. The critical work for heterogeneous cluster formation, ΔG_c^{het} [Eq. (7.19)], is obtained from Eq. (7.27b). Since nucleation is heterogeneous, ΔG_c^{het} is a lower limit for the critical work for homogeneous cluster formation ΔG_c [Eq. (7.4)].

Table 7.1 also shows the activation energy E_η of the shear viscosity η [Eq. (7.14)], which was obtained from stress relaxation experiments in thin films by wafer curvature measurements in a temperature range between 60 °C and 100 °C [7.53, 7.54]. According to Eq. (7.14), E_u and E_η should be equal under the assumption that the Stokes-Einstein equation [Eq. (7.12)] is valid for the phase change materials. However, since E_u is larger than E_η (Table 7. 1) and since the glass transition temperature T_g is usually accompanied by a discontinuity in activation energy (Fig. 7.3, activation energies above T_g are higher than below T_g), the data presented in Fig. 7.7 appear to be taken above T_g in the undercooled liquid. On the other hand, the viscosity was measured below T_g in the amorphous phase. T_g depends on the timescale of the experiment [7.19, 7.51] and should be significantly lower in the isothermal experiments (Figs. 7.7 and 7.8) than in a scanning experiment at constant heating rate of 40 K/min (Fig. 7.6). That the crystal growth velocity in Fig. 7.7 is time-independent points in the same direction: Only in the amorphous phase, but not in the undercooled liquid, would a time dependence of the atomic transport rates be expected due to structural relaxation (Fig. 7.3).

7.2.2 Crystallization Parameters Close to the Melting Temperature

Crystallization kinetics slightly below the melting temperature have rarely been investigated due to the high volatility of phase change materials at elevated temperatures (high vapor pressure of Sb and Te). However, in a recent study [7.19, 7.43], a lower limit for the crystal-melt interfacial free energy σ [Eq. (7.2)] and an upper limit for the *homo*geneous steady-state crystal nucleation rate I^{ss} [Eqs. (7.10) or (7.15)] was estimated by undercooling liquid droplets of phase change materials below the liquidus temperature T_l in a differential thermal analyzer (DTA) and measuring the undercooling, $\Delta T_n := (T_l - T_n) > 0$, at a constant cooling rate.[4] T_n is the temperature at which nucleation initiates upon cooling and was detected in the DTA by recalescence (re-heat of the droplet by the release of the heat of crystallization). Note that purely homogeneous nucleation gives the lowest possible nucleation rate, and that heterogeneities increase the nucleation rate substantially (Sect. 7.1.2). As a consequence, the undercooling ΔT_n is maximized for purely homogeneous nucleation, whereas the presence of any heterogeneity re-

[4] Since melting in alloys occurs over a range of temperatures, the liquidus temperature T_l is used instead of the melting temperature T_m in this section. T_l is the high-temperature end of the equilibrium melting range upon heating [7.19, 7.43, 7.56].

duces the value of ΔT_n. Therefore, in order to maximize ΔT_n and to approach the limit of homogeneous nucleation as closely as possible, the phase change material was embedded in a liquid flux of B_2O_3: This helped to isolate the droplet from the DTA crucible walls, which could act as heterogeneous nucleation sites. Additionally, B_2O_3 eliminates nucleants from the surface of the droplet by dissolution and inclusion [7.19, 7.43]. Moreover, the B_2O_3 prevented evaporation of the liquid volatile phase change material. Many heating and cooling cycles were performed in order to maximize ΔT_n further by additional fluxing. The undercooling data were then analyzed by *assuming* that the highest measured value for ΔT_n corresponds to the limit of *homo*geneous crystal nucleation. This substantially simplified the data analysis since $f(\theta)$ could be set to unity [Eq. (7.19)]. However, since it is unknown if this assumption is true, the obtained value for σ is only a *lower* limit for *homo*geneous nucleation, whereas the obtained curve for I^{ss} is only an *upper* limit for *homo*geneous nucleation (details: [7.19, 7.43]). Figure 7.9 shows the result.

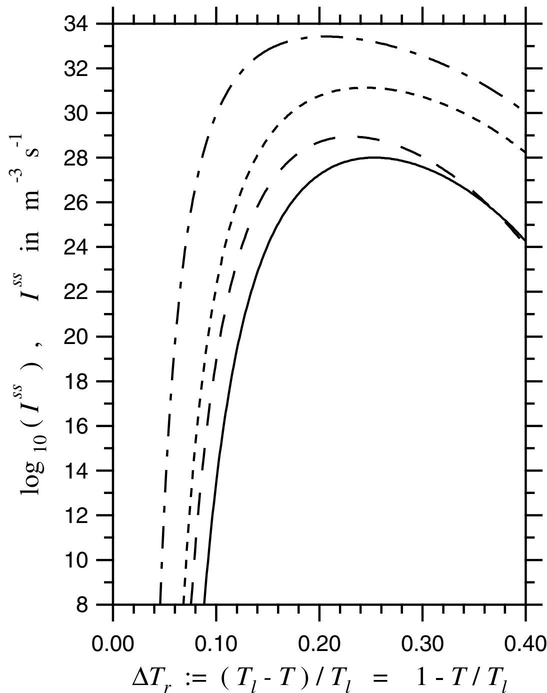

Fig. 7.9. Upper limit for the *homo*geneous steady state crystal nucleationrate I^{ss} [Eqs. (7.10) or (7.15)] as a function of *relative* undercooling $\Delta T_r := (T_l - T)/T_l$ for $Ge_2Sb_2Te_5$ (dot-dashed), $Ge_4Sb_1Te_5$ (dotted), $AgIn\text{-}Sb_2Te$ (dashed), and $Ge_{12}Sb_{88}$ (solid). T_l is the liquidus temperature. Reprinted with permission from [7.43]. Copyright [2005]. American Institute of Physics.

As explained in Sect. 7.1.1.4, the nucleation rate is negligibly small close to the melting (or liquidus) temperature, then increases rapidly upon cooling to a maximum, and then decreases again rapidly at the glass transition temperature T_g, which occurs (*relative* to the liquidus temperature) at $\Delta T_{rg} := 1 - T_g/T_l = 0.45$ - 0.55 depending on the alloy [7.19, 7.43, 7.51, 7.57]. The nucleation rates are

higher for the GeSbTe alloys, which exhibit nucleation-dominated crystallization [7.27], than for the Sb-rich alloys AgIn-Sb_2Te and $Ge_{12}Sb_{88}$, which exhibit growth-dominated crystallization [7.28, 7.29, 7.55]. This is a consequence of the fact that the Sb-rich alloys are characterized by a higher *relative* glass transition temperature, $T_{rg} = T_g/T_l$, and a higher entropy of fusion than the GeSbTe alloys (details: [7.19, 7.43, 7.51]).

The steady state nucleation rates in Fig. 7.9 are too high to allow amorphization in both optical and electronic phase change media under operating conditions. Nucleation interferes at the highest attainable cooling rates, which are on the order of 10^{10} Ks^{-1} [7.43, 7.58]. For optical data storage, the bit volume is on the order of $V_b = 1 \mu m \times 1 \mu m \times 10$ nm $=10^{-20}$ m^3 [7.59] (limited by the wavelength of the laser light). For a cooling rate of 10^{10} Ks^{-1}, the temperature decreases by 100 K during a time of $t_c := 10$ ns $= 10^{-8}$ s. Therefore, nucleation would interfere upon amorphization if the nucleation rate were $I^{ss} > V_b^{-1}\, t_c^{-1} = 10^{28}$ m^{-3} s^{-1} over a range of 100 K. This is certainly the case for the GeSbTe alloys, but most likely also for the Sb-rich alloys: Since the B_2O_3 flux has eliminated heterogeneous nucleation sites, the fluxing technique should have approached the limit of homogeneous nucleation (which gives the lowest possible nucleation rate) far closer than the nucleation rates in phase change media, for which heterogeneous nucleation is expected to dominate strongly due to the thin-film nature of the device. Moreover, nucleation in phase change media is frequently enhanced (i. e., heterogeneities are added) by nucleation-promoting dielectric capping layers [7.37, 7.60]. For electronic phase change media, programmable volume sizes as small as $V_b = 10^{-23}$ m^3 are reported [7.61, 7.62]. Hence, nucleation would interfere if $I^{ss} > 10^{31}$ m^{-3} s^{-1} over a range of 100 K, which is at least the case for $Ge_2Sb_2Te_5$, which is often reported as a prototypic material for phase change random access test devices [7.63]. Therefore, it can be concluded that:

1. Melt quenching under operating conditions occurs during the incubation time for crystal nucleation, when the steady-state cluster distribution N^{ss} (Fig. 7.2) is not yet formed, so that the nucleation rate remains far smaller than its steady state value I^{ss} [Eqs (7. 10), (7. 15) or (7. 20) [7.2, 7.24]]. As the incubation time is independent of the bit volume V_b, this statement applies equally to optical and electronic media for all alloys investigated. Consistently, it was reported by Kelton and Greer [7.64] that transient effects become increasingly important with increasing quench rate: While the steady state nucleation rate is readily maintained for cooling rates on the order of 1 K s^{-1} as used in the present experiments or in conventional metallurgical solidification, deviations from the steady state are already large at cooling rates in rapid solidification techniques, such as melt-spinning ($\sim 10^6$ K s^{-1}), and must be even larger for cooling rates on the order of 10^{10} K s^{-1} which occur under operating conditions of phase change media.
2. Amorphization would not be possible if the incubation time for crystal nucleation were absent. Hence, the existence of an incubation time makes phase change recording possible. This statement should apply for optical data stor-

age to all alloys investigated and for electronic data storage at least to $Ge_2Sb_2Te_5$. Indeed, incubation times were reported upon crystallization on the timescale of minutes around T_g [7.36, 7.40, 7.41, 7.48], as well as upon laser crystallization on the nanosecond timescale [7.27, 7.30, 7.65-7.67].

Acknowledgement. Frans Spaepen is gratefully acknowledged for critical proof-reading and valuable input to this chapter.

References

[7.1] Gibbs, J.: The scientific papers of J. Willard Gibbs. Dover Publications, New York (1961)
[7.2] Christian, J.: Transformation in metals and alloys, 2nd edn. Pergamon Press, Oxford (1975)
[7.3] Kelton, K.: Crystal nucleation in liquids and glasses. Solid State Physics **45**, 75-177 (1991)
[7.4] Volmer, M. and Weber, A.: Keimbildung in übersättigten Gebilden. Zeitschrift für Physikalische Chemie **119**, 277 (1926)
[7.5] Becker, R. and Döring, W.: Kinetische Behandlung der Keimbildung in übersättigten Dämpfen. Annalen der Physik **24**, 719 (1935)
[7.6] Turnbull, D. and Fisher, J.: Rate of nucleation in condensed systems. J. Chem. Phys. **17**, 71-73 (1949)
[7.7] Landau, L. and Lifshitz, E.: Statistical Physics. Pergamon Press, Oxford (1969)
[7.8] Thompson, C. and Spaepen, F.: Homogeneous crystal nucleation in binary metallic melts. Acta Metallurgica **31**, 2021-2027 (1983)
[7.9] Herlach, D.: Non-equilibrium solidification of undercooled metallic melts. Materials Science and Engineering R **12**, 177-272 (1994)
[7.10] Angell, C., Ngai, K., McKenna, G., McMillan, P. and Martin, S.: Relaxation in glass-forming liquids and amorphous solids. J. Appl. Phys. **88**, 3113-3157 (2000)
[7.11] Debenedetti, P. and Stillinger, F.: Supercooled liquids and the glass transition. Nature **410**, 259-267 (2001)
[7.12] Götze, W.: Liquids, freezing and the glass transition. Les Houches LI. North-Holland, Amsterdam (1991), p. 287
[7.13] Hodgdon, J. and Stillinger, F.: Stokes-Einstein violation in glass-forming liquids. Phys. Rev. E **48**, 207-213 (1993)
[7.14] Shao, Y. and Spaepen, F.: Undercooling of bulk liquid silicon in an oxide flux. J. App. Phys. **79**, 2981-2985 (1996)
[7.15] Spaepen, F.: The identification of the metallic glass state. In: Mat. Res. Soc. Symp. Proc., vol. **57**, p. 161-184 (1986)
[7.16] Thompson, C., Greer, A. L. and Spaepen, F.: Crystal nucleation in amorphous $(Au_{100-y}Cu_y)_{77}Si_9Ge_{14}$ alloys. Acta Metallurgica **31**, 1883-1894 (1983)
[7.17] Turnbull, D.: Kinetics of solidification of supercooled liquid mercury droplets. J. Chem. Phys. **20**, 411-424 (1952)

[7.18] Turnbull, D.: Under what conditions can a glass be formed? Contemp. Phys. **10**, 473-488 (1969)
[7.19] Kalb, J.: Crystallization kinetics in antimony and tellurium alloys used for phase change recording. Ph.D. thesis, RWTH Aachen, Germany (2006). URL www.kalb.eu/publications
[7.20] Spaepen, F.: Physics of Defects. Les Houches XXXV. North-Holland, Amsterdam (1981), pp. 133-174
[7.21] Spaepen, F. and Turnbull, D.: Metallic glasses. Ann. Rev. Phys. Chem. **35**, 241-263 (1984)
[7.22] Elliott, S.: Physics of amorphous materials, 2nd edn. Longman, London (1990)
[7.23] Volmer, M.: Über Keimbildung und Keimwirkung als Spezialfälle der heterogenen Katalyse. Zeitschrift für Elektochemie **35**, 555 (1929)
[7.24] Wu, D.: Nucleation theory. Solid State Physics **50**, 37-187 (1997)
[7.25] Holland-Moritz, D.: Short-range order and solid-liquid interfaces in undercooled melts. Int. Journ. Non-Equilibrium Processing **11**, 169-199 (1998)
[7.26] Crank, J.: The mathematics of diffusion, 2nd edn. Clarendon Press, Oxford (1975)
[7.27] Coombs, J., Jongenelis, A., van Es-Spiekman, W. and Jacobs, B.: Laser-induced crystallization phenomena in GeTe-based alloys. II. Composition dependence of nucleation and growth. J. Appl. Phys. **78**, 4918-4928 (1995)
[7.28] van Pieterson, L., Lankhorst, M., van Schijndel, M., Kuiper, A. and Roosen, J.: Phase-change recording materials with a growth-dominated crystallization mechanism: A materials overview. J. Appl. Phys. **97**, 083520 (2005)
[7.29] van Pieterson, L., van Schijndel, M., Rijpers, J. and Kaiser, M.: Te-free, Sb-based phase-change materials for high-speed rewritable optical recording. Appl. Phys. Lett. **83**, 1373-1375 (2003)
[7.30] Weidenhof, V., Friedrich, I., Ziegler, S. and Wuttig, M.: Laser induced crystallization of amorphous $Ge_2Sb_2Te_5$ films. J. Appl. Phys. **89**, 3168-3176 (2001)
[7.31] Yamada, N., Ohno, E., Nishiuchi, K., Akahira, N. and Takao, M.: Rapid phase transitions of GeTe-Sb_2Te_3 pseudobinary amorphous thin films for an optical disk memory. J. Appl. Phys. Physics **69**, 2849-2856 (1991)
[7.32] Friedrich, I., Weidenhof, V., Njoroge, W., Franz, P. and Wuttig, M.: Structural transformations of $Ge_2Sb_2Te_5$ films studied by electrical resistance measurements. J. Appl. Phys. **87**, 4130-4134 (2000)
[7.33] Jeong, T., Kim, M., Seo, H., Kim, S. and Kim, S.: Crystallization behavior of sputter-deposited amorphous $Ge_2Sb_2Te_5$ thin films. J. Appl. Phys. **86**, 774-778 (1999)
[7.34] Kooi, B. and De Hosson, J.: On the crystallization of thin films composed of $Sb_{3.6}Te$ with Ge for rewritable data storage. J. Appl. Phys. **95**, 4714-4721 (2004)
[7.35] Libera, M. and Chen, M.: Time-resolved reflection and transmission studies of amorphous Ge-Te thin-film crystallization. J. Appl. Phys. **73**, 2272-2282 (1993)
[7.36] Lu, Q. and Libera, M.: Microstructural measurements of amorphous GeTe crystallization by hot-stage optical microscopy. J. Appl. Phys. **77**, 517-521 (1995)
[7.37] Njoroge, W., Dieker, H. and Wuttig, M.: Influence of dielectric capping layers on the crystallization kinetics of $Ag_5In_6Sb_{59}Te_{30}$ films. J. Appl. Phys. **96**, 2624-2627 (2004)
[7.38] Njoroge W. and Wuttig, M.: Crystallization kinetics of sputter-deposited amorphous AgInSbTe films. J. Appl. Phys. **90**, 3816 (2001)
[7.39] Pedersen, T.L., Kalb, J., Njoroge, W., Wamwangi, D., Wuttig, M. and Spaepen, F.: Mechanical stresses upon crystallization in phase change materials. Appl. Phys. Lett. **79**, 3597-3599 (2001)
[7.40] Privitera, S., Bongiorno, C., Rimini, E. and Zonca, R.: Crystal nucleation and growth processes in $Ge_2Sb_2Te_5$. Appl. Phys. Lett. **84**, 4448-4450 (2004)
[7.41] Ruitenberg, G., Petford-Long, A. and Doole, R.: Determination of the isothermal nucleation and growth parameters for the crystallization of thin $Ge_2Sb_2Te_5$ films. J. Appl. Phys. **92**, 3116-3123 (2002)

[7.42] Wamwangi, D., Njoroge, W. and Wuttig, M.: Crystallization kinetics of $Ge_4Sb_1Te_5$ films. Thin Solid Films **408**, 310-315 (2002)
[7.43] Kalb, J., Spaepen, F. and Wuttig, M.: Kinetics of crystal nucleation in undercooled droplets of Sb-and Te-based alloys used for phase change recording. J. Appl. Phys. **98**, 054910 (2005)
[7.44] Kissinger, H.: Reaction kinetics in differential thermal analysis. Analyt. Chem. **29**, 1702 (1957)
[7.45] Avrami, M.: Kinetics of phase change. I. General theory. J. Chem. Phys. **7**, 1103-1112 (1939)
[7.46] Johnson, W. and Mehl, R.: Reaction kinetics in process of nucleation and growth. Trans. Amer. Inst. of Mining, Metallurgical and Petroleum Engineers **135**, 416 (1939)
[7.47] Kalb, J., Spaepen, F. and Wuttig, M.: Atomic force microscopy measurements of crystal nucleation and growth rates in thin films of amorphous Te alloys. Appl. Phys. Lett. **84**, 5240-5242 (2004)
[7.48] Kalb, J., Wen, C., Spaepen, F., Dieker, H. and Wuttig, M.: Crystal morphology and nucleation in thin films of amorphous Te alloys used for phase change recording. J. Appl. Phys. **98**, 054902 (2005)
[7.49] Kooi, B., Groot, W. and De Hosson, J.: In situ transmission electron microscopy study of the crystallization of $Ge_2Sb_2Te_5$. J. Appl. Phys. **95**, 924-932 (2004)
[7.50] Weidenhof, V., Friedrich, I., Ziegler, S. and Wuttig, M.: Atomic force microscopy study of laser induced phase transitions in $Ge_2Sb_2Te_5$. J. Appl. Phys. **86**, 5879-5887 (1999)
[7.51] Kalb, J., Wuttig, M. and Spaepen, F.: Calorimetric measurements of structural relaxation and glass transition temperatures in sputtered films of amorphous Te alloys used for phase change recording. J. Mater. Res. **22**, 748-754 (2007)
[7.52] Spaepen, F.: Private communication
[7.53] Kalb, J.: Stresses, viscous flow and crystallization kinetics in thin films of amorphous chalcogenides used for optical data storage. Diploma thesis, RWTH Aachen, Germany (2002). URL www.kalb.eu/publications
[7.54] Kalb, J., Spaepen, F., Pedersen, T.L. and Wuttig, M.: Viscosity and elastic constants of thin films of amorphous Te alloys used for optical data storage. J. Appl. Phys. **94**, 4908-4912 (2003)
[7.55] Borg, H., van Schijndel, M., Rijpers, J., Lankhorst, H., Zhou, G., Dekker, M., Ubbens, I. and Kuijper, M.: Phase-change media for high-numerical-aperture and blue-wavelength recording. Jpn. J. Appl. Phys. **40**, Part 1, 1592-1597 (2001)
[7.56] Shackelford, J.: Introduction to Materials Science for Engineers, 2nd edn. Macmillan, New York (1988)
[7.57] Kalb, J., Spaepen, F. and Wuttig, M.: Calorimetric measurements of phase transformations in thin films of amorphous Te alloys used for optical data storage. J. Appl. Phys. **93**, 2389-2393 (2003)
[7.58] Peng, C., Cheng, L. and Mansuripur, M.: Experimental and theoretical investigations of laser-induced crystallization and amorphization in phase-change optical recording media. J. Appl. Phys. **82**, 4183-4191 (1997)
[7.59] Kaiser, M., van Pieterson, L. and Verheijen, M.: In situ transmission electron microscopy analysis of electron beam induced crystallization of amorphous marks in phase-change materials. J. Appl. Phys. **96**, 3193-3198 (2004)
[7.60] Ohshima, N.: Crystallization of germanium-antimony-tellurium amorphous thin film sandwiched between various dielectric protective films. J. Appl. Phys. **79**, 8357-8363 (1996)
[7.61] Haring-Bolivar, P., Merget, F., Kim, D.H., Hadam, B. and Kurz, H.: European Symposium on Phase Change and Ovonic Science (EPCOS), Balzers, Liechtenstein, unpublished (2004)
[7.62] Lankhorst, M., Ketelaars, B., Wolters, R.: Low-cost and nanoscale non-volatile memory concept for future silicon chips. Nature Materials **4**, 347-352 (2005)

[7.63] Hudgens, S. and Johnson, B.: Overview of phase-change chalcogenide nonvolatile memory technology. Materials Research Society Bulletin **29**, 829-832 (2004)
[7.64] Kelton, K., Greer, A.: Transient nucleation effects in glass formation. Journal of Non-Crystalline Solids **79**, 295-309 (1986)
[7.65] Friedrich, I., Weidenhof, V., Lenk, S. and Wuttig, M.: Morphology and structure of laser-modified $Ge_2Sb_2Te_5$ films studied by transmission electron microscopy. Thin Solid Films **389**, 239-244 (2001)
[7.66] Wöltgens, H.W., Detemple, R., Friedrich, I., Njoroge, W., Thomas, I., Weidenhof, V., Ziegler, S. and Wuttig, M.: Exploring the limits of fast phase change materials. In: Materials Research Society Symposia Proceedings, vol. **674**, p. V1.3 (2001)
[7.67] Ziegler, S.: Rekristallisationskinetik von Phasenwechselmedien. Ph.D. thesis, RWTH Aachen, Germany (2005)

Author Bios

Dr. Simone Raoux, IBM Almaden Research Center, 650 Harry Road, San Jose, CA 95120, USA. She is Research Staff Member at the IBM Almaden Research Center. She received her MS degree in 1984 and Ph.D. degree in physics in 1988 from Humboldt University, Berlin, Germany. Before joining IBM she worked at the Institute for Electron Physics, Berlin, and Lawrence Berkeley National Laboratory, Berkeley, CA. Her current research interests include the physics and materials science of phase change materials.

Prof. Matthias Wuttig, 1. Physikalisches Institut (1A), RWTH Aachen University, 52056 Aachen, Germany. He received his diploma from Cologne (1986) and Ph.D. from Aachen University (1988). He is a Full Professor of Physics at RWTH Aachen since 1997 and is presently Dean of the Faculty of Mathematics, Computer Science and the Natural Sciences. As a visiting scientist he has worked at NIRIM Tsukuba (Japan), Bell Labs (USA), CRMC^2 Marseille (France), Zhejiang University (China), IBM Research Center and UC Berkeley (USA). His main interest is the development of novel materials.

Dr. Stanford R. Ovshinsky, Ovshinsky Innovation LLC, 1050 East Square Lake Road, Bloomfield Hills, MI 48304, USA. He is the co-founder of Energy Conversion Devices, Inc. (ECD) and is the primary inventor of ECD's technology including the Ovonic Universal Memory (OUM), the Ovonic optical memory and various other chalcogenide devices, Ovonic thin-film photovoltaic technology and its continuous web multi-junction roll-to-roll machine, the Ovonic NiMH battery which enabled the electric and hybrid automotive industry, as well as the Ovonic solid hydrogen storage technology. He started the field of amorphous and disordered materials in the 1950s by atomically designing devices that have unique electronic, chemical and structural mechanisms. In 2007 he formed an independent new company called *Ovshinsky Innovation LLC*.

Dr. Chung Lam, T. J. Watson Research Center, Yorktown Heights, NY 10598, USA. He received his B.Sc. in Electrical Engineering at Polytechnic University of New York in 1978, and joined IBM General Technology Division in Burlington in 1978 as a memory circuit designer. In 1984, he was awarded the IBM Resident Study Fellowship and received his M.Sc. and Ph.D., both in Electrical Engineering, at Rensselaer Polytechnic Institute in 1987 and 1988 respectively. In 2003, Dr. Lam transferred to IBM Research Division, and was named Distinguished Engineer in 2007. He has managed the Phase-change memory Research Project at the IBM Research Division in T.J. Watson Research Center since 2003.

Dr. Wojciech Welnic, Laboratoire des Solides Irradies, Ecole Polytechnique, 91128 Palaiseau, France. He received his Ph.D. in 2006 from the Technical University Aachen working on phase change materials. He spent time at the Forschungszentrum, Juelich, Germany and the Ecole Polytechnique in Paris, France to study computational methods in solid state physics. He is currently a postdoctoral fellow at the Ecole Polytechnique and the ESRF in Grenoble working on electronic and structural properties of phase change materials.

Prof. Punit Boolchand, University of Cincinnati, 820 Rhodes Hall, Cincinnati, OH 45221-0030, USA. He received his Ph.D. in Physics from Case-Western Reserve University in 1969. He is currently a Professor of Electrical and Computer Engineering, and Physics at University of Cincinnati. He has been interested in nature of glass transition and molecular structure of network glasses probed by thermal, optical, nuclear and electrical methods. He has held visiting positions at Stanford (USA), Univ. of Paris VI (France), Leuven University (Belgium). He is a Fellow of the American Physical Society.

Prof. Matthieu Micoulaut, Laboratoire de Physique Théorique de la Matière Condensée, CNRS UMR 7600 Université Pierre et Marie Curie, Boite 121, 4 place Jussieu 75252 Paris Cedex 05, France. He received his Ph.D. in Theoretical Physics from University Paris VI (1993). He is currently Maitre de Conférences (Associate Professor) in theory of condensed matter (CNRS and UPMC-Paris VI). His interests include theoretical aspects of glass transition, glasses and amorphous solids, and topology based approaches and molecular simulations to investigate structure and dynamics of supercooled liquids.

Ping Chen, Department of Electrical and Computer Engineering, University of Cincinnati, Cincinnati, OH 45221-0030, USA. He received his M.S. degree in Microelectronics from Nanjing University (2002). He is currently graduate student in the Department of Electrical and Computer Engineering at University of Cincinnati and working towards his Ph.D. degree. He is interested in molecular structure, reversibility window and aging in alkali-germanate and As-chalcogenide glasses.

Prof. Stephen Elliott, Department of Chemistry, University of Cambridge, Lensfield Road, Cambridge CB2 1EW, UK. He is Professor of Chemical Physics in the Department of Chemistry, and a Fellow of Trinity College, at the University of Cambridge. His research interests centre on studies of disordered materials, particularly chalcogenide glasses, from both experimental and theoretical/computer-simulation points of view. He was the recipient, in 2001, of the first Ovshinsky Prize for research on chalcogenide materials.

Dr. Liesbeth van Pieterson, Philips Research, High Tech Campus 4 (Box WAG 12), 5656 AE Eindhoven, The Netherlands. She received her PhD degree in chemistry of condensed matter from Utrecht University in 2001. She is a senior scientist at Philips Research Laboratories in The Netherlands. Her research interest is in the area of solid-state chemistry with a current focus on the physics and chemistry of materials for optical recording.

Dr. Johannes Kalb, Intel Corporation, Robert Noyce Building, Mail Stop RNB-3-01, 2200 Mission College Blvd., Santa Clara, CA 95054, USA. He received his MS (2002) and PhD degree (2006) from the Technical University of Aachen, Germany. As a graduate student, he spent two years at the School of Engineering and Applied Sciences at Harvard University, working on stresses and crystallization kinetics in phase change materials. In 2006 he joined the Department of Materials Science and Engineering at MIT as a Postdoctoral Researcher. Since 2007 he has been with Intel Corporation, continuing research on phase change materials.

Dr. Paul Fons, Advanced Institute of Industrial Science and Technology, Tsukuba, Japan. He received a masters in physics and a Ph.D. in materials science from the University of Illinois, graduating in 1990. He was visiting research fellow at the Applied Physics Department of the University of Tsukuba in Japan. He became a permanent staff member of the Optoelectronics division of the Electrotechnical Laboratory of AIST in 1993. In 2003, he moved to the Center for Applied Near-Field Optics Research to work on materials characterization of optical disk materials where he is now head of the Nano Optics research group.

Dr. Bong-Sub Lee, University of Illinois at Urbana-Champaign, 1-110 Engineering Sciences Building, 1101 W. Springfield Ave., Urbana, IL 61801, USA. He is a post-doctoral research associate at the University of Illinois at Urbana-Champaign, where he received his Ph. D. in Materials Science and Engineering in 2006. He received his M.S. and B.S. (cum Laude) at Seoul National University, Korea. He is a winner of the E*PCOS 07 Presentation Award, European Phase Change and Ovonics Symposium (2007), as well as other awards and scholarships.

Prof. Stephen Bishop, University of Illinois at Urbana-Champaign, 153 Everitt Laboratory, 1406 West Green St, MC-702, Urbana, IL 61801, USA. He is Professor of Electrical and Computer Engineering and Physics at the University of Illinois at Urbana-Champaign (UIUC). Before joining the UIUC in 1989, he was a research physicist for 23 years at the Naval Research Laboratory (NRL) in Washington, D.C. He received his BA from Gettysburg College and a Ph.D. in physics from Brown University.

Dr. Noboru Yamada, AV Core Technology Development Center, Matsushita Electric Industrial Co., Ltd. (Panasonic), 3-1-1 Yagumo-Nakamachi, Moriguchi, Osaka, Japan. He graduated in Electronic Science and Engineering in 1974 and obtained a Ph.D. in Engineering in 2001, both from Kyoto University. He joined Matsushita Electric Ind. Co., Ltd. in 1974. Since then he has been working in the Corporate R&D division. He was the first to propose GeTe-Sb_2Te_3 phase-change materials in 1987 and he pioneered several optical disc media such as DVD-RAMs and Dual layer Blu-ray discs using this material. Currently, he is General Manager of the Storage Media Group, AV Core Technology Development Center.

Dr. Delia J. Milliron, The Molecular Foundry, Lawrence Berkeley National Laboratory, 1 Cyclotron Road, Berkeley, CA 94720, USA. She is the Facility Director for Inorganic Nanostructures at the Molecular Foundry, and was previously a Research Staff Member at IBM. She obtained her A.B. from Princeton University in 1999 and her Ph.D. from the University of California, Berkeley in 2004, both in Chemistry. Her research interests include chemical synthesis and materials integration of colloidal nanoparticles and solution deposition of metal chalcogenide thin films.

Dr. Qiang Huang, IBM T. J. Watson Research Center, P. O Box 218, Yorktown Heights, NY 10598, USA. He is Research Staff Member at the IBM TJ Watson Research Center. He obtained his B.E. from Zhejiang University in 1997, and his PhD from Louisiana State University in 2004, both in Chemical Engineering. His research interest includes Cu interconnects, electrodeposition of semiconductor materials, magnetic alloys, nanomaterials and nanodevices.

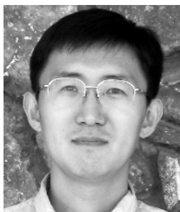

Dr. Yu Zhu, IBM T. J. Watson Research Center, P.O.Box 218, Yorktown Heights, NY 10598, USA. He is advisory engineer at IBM TJ Watson Research Center. He obtained his Ph.D. from College of Nanoscale Science and Engineering of University at Albany – SUNY. His research interests include atomic layer deposition and chemical vapor deposition of thin films for electronic device application.

Dr. Luping Shi, Data Storage Institute, DSI Building, 5 Engineering Drive 1, Singapore 117608. He received a master degree in solid physics from Shan Dong University, P.R. China in 1988, and doctor of science degree from Cologne University, Germany, in 1992. He joined the Data Storage Institute (DSI), Singapore, in 1996 as a Senior Engineer. Currently, he is senior Research Scientist, division manager of the Optical Materials & System division. He is in charge of optical storage, solid state random access memory (PCRAM) and artificial cognitive sensor and memory researches at DSI.

Dr. Junji Tominaga, Center for Applied Near-Field Optics Research, CAN-FOR, National Institute of Advanced Industrial Science & Technology, Tsukuba Central #4, 1-1-1 Higashi, Tsukuba, 305-8562, Japan. He received his Ph. D. from Cranfield Univ. UK in 1991. After research on rewritable optical phase-change disks at TDK corporation, he moved to the National Institute of Advanced Industrial Science & Technology (AIST) in 1997. He is currently director of the Center for Applied Near-Field Optics Research and has been the leader of the super-RENS ultra-high density optical storage project.

Prof. Daniele Ielmini, Dipartimento di Elettronica e Informazione, Politecnico di Milano, piazza Leonardo da Vinci 32, 20133 - Milano (MI), Italy. He received the Laurea (cum laude) and the Ph. D. degrees from the Politecnico di Milano, Italy in 1995 and 1999, respectively. He has been an Assistant Professor at Dipartimento di Elettronica e Informazione, Politecnico di Milano, since 2002. His main research interest is characterization and modelling of non volatile memories, including Flash, discrete-trap, phase-change and resistive-switching memories.

Dr. Yi-Chou Chen, Emerging Central Lab, Macronix Int. Co., Ltd., 16 Li-Hsin Road, Science Park, Hsinchu, Taiwan. He received his B.S. degree and Ph.D. degree in chemical engineering in 1995 and 2000, respectively, both from National Taiwan University. In 2000, he joined Macronix and worked on technology development of lithography, moving to the Emerging Central Lab in 2001 where he started working on phase change memory. From 2005 to 2007, he was on assignment at the IBM Almaden Research Center. His current research interests include both phase change material and memory devices.

Dr. Roberto Bez, STMicroelectronics M6 s.r.l. (at the time of publication with Numonyx), Via C.Olivetti 2, 20041, Agrate Brianza, Milan, Italy. He received the doctor degree in physics from the University of Milan, Italy, in 1985. In 1987 he joined STMicroelectronics and since then has worked on the Non-Volatile Memory technology development in the R&D department. He has been director of the Phase Change Memory, in the NVM Technology Development. He has authored many papers, conference contributions and patents on topics related to NVM and been lecturer on Non-Volatile Memory Devices at many Italian universities.

Dr. Robert J. Gleixner, Intel Corp. (at the time of publication with Numonyx), 2200 Mission College Blvd., Santa Clara, California. He received his Ph.D. degree in materials science from Stanford University in 1998. He joined Intel's Corporate Quality and Reliability group in 1998 and has worked on microprocessor, microdisplay, and non-volatile memory technologies and products. Since 2004, his work has focused on developing and productizing advanced Phase Change Memory technologies.

Dr. Fabio Pellizzer, STMicroelectronics M6 s.r.l. (at the time of publication with Numonyx), Via C.Olivetti 2, 20041, Agrate Brianza, Milan, Italy. He received the doctor degree in electronic engineering in 1996 from the University of Padova, Italy, with a thesis on characterization and reliability of thin gate oxides. In 1998 he joined the Central R&D department of STMicroelectronics in Agrate Brianza (Italy). After 2002 he has been in charge of process development for phase-change memories based on chalcogenide materials. He has authored many papers, conference contributions, and patents on phase-change memories.

Dr. Agostino Pirovano, STMicroelectronics M6 s.r.l. (at the time of publication with Numonyx), Via C.Olivetti 2, 20041, Agrate Brianza (Milan), Italy. He received the Laurea degree in electrical engineering from the Politecnico di Milano, Italy, in 1997, and the Ph.D. degree at the Department of Electrical Engineering, Politecnico di Milano, Italy, in 2000. Since 2001 he has worked on the electrical characterization and modeling of phase-change memories. In 2003 he joined the Non-Volatile Memory Technology Development Group of STMicroelectronics and he has been involved in the investigation of PCM and of emerging NVM technologies.

Dr. Greg Atwood, Intel Corp. (at the time of publication with Numonyx), 2200 Mission College Blvd., Santa Clara, California. He received the master degree in physics from Purdue University in 1979 at which time he joined Intel working initially in Micro-Processor technology development and latter in Non-Volatile Memory technology development, achieving the appointment of Intel Fellow in 1996. Since 2000, his primary focus has been on Phase Change Memory Technology and its application to electrical Non-Volatile Memories.

Dr. Matthew Breitwisch, IBM T. J. Watson Research Center, P. O Box 218, Yorktown Heights, NY 10598, USA. He is Research Staff Member at the IBM T.J. Watson Research Center in Yorktown Heights, NY. He received his B.S. degree in physics, mathematics, and astrophysics from the University of Wisconsin at Madison in 1994, and a Ph.D. degree in physics from Iowa State University in 1999. He joined IBM at the Microelectronics Center in Essex Junction, VT, and since 2005 has worked in the IBM Research exploratory memory group focusing on integration schemes for phase change memory devices.

Dr. James Lyke Air Force Research Laboratory (AFRL/RVSE), 3550 Aberdeen Ave SE, KAFB, NM 87117-5776, USA. He has a BS from the University of Tennessee, Knoxville, an MS from the Air Force Institute of Technology, and a PhD through the University of New Mexico, all in electrical engineering. He serves as technical advisor to the Space Electronics Branch of the Air Force Research Laboratory's Space Vehicles Directorate (AFRL/VSSE) at Kirtland Air Force Base New Mexico. His primary pursuits are the development of novel space systems architectures, especially those exploiting reconfigurable / plug-and-play approaches. He also maintains a keen interest in 3-D packaging and molecularly-scalable computational approaches.

Index

A

Ab initio, 17, 24, 25, 26, 27, 29, 32, 36, 68, 72, 74, 78, 292, 326
Ab initio molecular dynamics, 24, 25, 26, 27, 68, 72, 74, 78
Absorption coefficient, 176
Accelerated bake testing, 369
Access device, 100, 332, 381, 382, 383, 384, 388, 390–392, 398, 401, 403, 406
Activation energies, 48, 95, 104, 113, 131, 137, 141, 142, 194, 319, 323, 324
  of crystallization, 84, 90, 95, 110, 113, 114, 138, 269, 342, 371
  of crystal nucleation rate and crystal growth velocity, 138
Adhesion layer, 334–335
Aging, 41, 44, 50, 52, 53, 268, 420
AgInSbTe, 94, 215, 216, 263, 264, 266, 279
ALD, *see* Atomic layer deposition (ALD)
Alkali silicates, 54
Amorphization, 25, 34, 35, 36, 82, 93, 113, 119, 144, 156, 157, 178, 204, 207, 260, 261, 262, 266, 267, 310
Amorphous, as-deposited material, 105, 106
Amorphous materials, 63, 64, 65, 66, 68, 72, 149, 203, 320, 321
Amorphous, melt-quenched material, 106
Amorphous phase stability, 86, 89, 91, 93, 96
Amorphous stability, 94, 200, 204
Antibonding, 31, 32, 324
Archival life stability, 81, 82, 89–91, 95
Arrhenius, 43, 44, 46, 56, 95, 130, 131, 140, 141, 302, 315, 317, 318, 319, 320, 324, 370, 371, 372
  plot, 95, 302, 317, 318, 371
Atomic displacement, 157, 215, 217, 218
Atomic force microscopy, 138, 230, 231
Atomic layer deposition (ALD), 100, 230, 237
Atomic models, 68
Atomic scattering factor, 67
Atomic vacancies, 74, 76
AWSAM, 273

B

Bake, 239, 321, 369, 370, 372, 373, 374, 376
Band gap, 23, 31, 33, 184, 194, 195, 202, 292, 309
BD, 81, 211, 219, 220, 252, 253, 256, 257, 258, 259, 271, 274, 279, 280, 286, 287, 290
Becker-Döring model for crystal nucleation, 128, 129
Bipolar junction transistor (BJT), 356, 357, 364, 383, 391, 392
  based cell, 391
Birefringence, 54
Bit error rate, 272, 273
Blu-ray, 81, 89, 97, 108, 209, 219, 221, 252, 256, 257, 286
  discs, 81, 89, 97, 209, 221, 256, 257
Bond
  angle(s), 27, 64, 65, 218
    distribution, 73, 74, 76, 77, 78
  length, 26, 47, 64, 65, 67, 68, 70, 71, 73, 76, 77, 78, 164, 165, 168, 169, 170, 217, 286
Bond-bending constraints, 46
Born-Oppenheimer approximation, 18
Bottom electrode, 231, 233, 300, 301, 308, 309, 310, 311, 312, 313, 320, 332, 338, 342, 344, 349, 350, 382, 385, 393, 394, 395, 396, 397, 399, 401
Breakdown characteristic, 1
Bridge structure, 341, 342–343
Burstein-Moss shift, 181, 192

C

Capping layers, 102, 104, 144, 265
Carbohydrates, 57, 58
Car-Parrinello (CP), 74
Carrier concentration, 184, 187, 188, 189, 192, 193
CD-ROM, *see* Compact Disc-Read Only Memory (CD-ROM)
Cell
  failure(s), 371, 372, 373, 375
  placement algorithms, 378
CET, *see* Complete erasing times (CET)
Chalcogenide(s), 1, 3, 4, 5, 43, 45, 47, 51, 58, 81, 149, 151, 152, 154, 182, 183, 184, 185, 188, 194, 199, 200, 201, 202, 234, 235, 238, 240, 243, 265, 286, 288, 290, 291, 293, 296, 299, 300, 302, 306, 307, 308, 309, 310, 311, 312, 313, 315, 320, 322, 326, 343, 356, 357, 358, 364, 365, 369, 377, 378, 379, 423, 424, 425, 426
  semiconductors, 199, 200, 201, 202–203
Chalcohalide, 45, 46
Chalcopyrite, 32
Chemical bond-strength scaling, 48
Chemical disorder, 65
Chemical Mechanical Polishing (CMP), 333, 339, 340, 342, 346, 396, 398, 399
Chemical Orbital Hamilton Population (COHP), 31, 32
Chemical threshold, 50
Chemical vapor deposition (CVD), 227–233, 238, 241, 243, 244, 345, 346, 393, 396, 399, 400, 401, 403
  pulsed, 230
CMP, *see* Chemical Mechanical Polishing (CMP)
COHP, *see* Chemical Orbital Hamilton Population (COHP)
Collar process, 396, 399, 400, 401
Collision-limited crystallization, 129, 130
Compact Disc (CD), 81, 176, 194, 252, 253, 257, 258, 259, 271, 285, 287, 333, 339, 397, 398, 399, 400, 401, 402
Compact Disc-Read Only Memory (CD-ROM), 252, 253, 254, 259
Compact Disc–Recordable (CD-R), 252, 253, 254, 285
Compact Disc – ReWritable (CD-RW), 81, 94, 220, 252, 253, 254, 259, 285
Complete crystallizing time, 264
Complete erasing times (CET), 105, 106, 264
Composition triangle, 85, 86
Compound composition, 207, 212, 266
Computational phase transitions, 40
Conduction activation energy, 194, 304
Confined structure, 345–346, 350, 398
Conformal deposition profile, 227
Contact-minimized, 397, 399
Coordination number(s), 28, 41, 46, 47, 50, 51, 56, 65, 67, 68, 71, 72, 73, 75, 94, 129, 160, 165
Critical radius for crystal nucleation, 127, 134
Cross-linking, 50, 54, 203
Cross-spacer structure, 344
Crystal
  growth
    speed, 206
    velocity, 96, 106, 136, 137, 138, 139, 140, 141, 142
  nucleation rate, 138, 139, 140, 141, 142
Crystallization
  activation energy, 84, 90, 95, 110, 113, 114, 138, 269, 342, 371
  behavior of nanoparticles, 115, 117, 118
  mechanism, 85, 86, 87, 88, 89, 94, 106, 141, 270, 323, 334, 372, 389
  rate, 81, 87, 88, 91–93, 94, 95, 96, 100, 105–107, 150, 204
  speed, 92, 99, 100, 104, 106, 107, 110, 118, 199, 204, 205, 207, 218, 221, 262, 265, 276, 277, 278, 334, 341, 342, 343, 389
  temperature, 82, 94, 95, 99, 100, 101, 102, 103, 104, 106, 110, 115, 117, 118, 138, 204, 206, 208, 211, 212, 221, 230, 231, 239, 242, 261, 265, 266, 278, 357, 384, 385, 386, 389
  times, 32, 96, 119, 153, 154, 314
Cubic phase, 152, 153, 154, 209, 213, 214, 216, 223
Current crowding effect, 334
Current – voltage characteristics, 4, 368, 385
CVD GST, 230, 231, 233, 400, 401
CVD, *see* Chemical vapor deposition (CVD)

Cyclability, 199, 205, 206, 213, 215, 232, 260, 265, 270
Cycle numbers, 206, 211
Cycle times, 199
Cycling, 113, 368, 374, 377–378, 390

D

3-D, 403
Dangling ends, 45
Data mining, 29
Data retention, 101, 113, 114, 199, 232, 242, 266, 299, 314, 326, 334, 336, 341, 361, 368, 369, 370, 371, 374, 375, 376
Degenerate semiconductor, 181, 192, 193
Demix, 40, 47, 53, 54
Density functional theory (DFT), 17–36
Density of states, 24, 31, 33, 34, 35, 47, 71, 181
Device design, 188, 228, 243, 381, 390, 393
Dielectric function, 34
Differential scanning calorimetry, 27, 39, 42, 48, 101, 139, 154, 213, 321, 323
Differential thermal analysis, 142
Diffraction limit, 257, 271, 279, 286–288, 289, 290, 291, 295
Diffusion-limited crystallization, 129, 132
Diffusion, long range, 129, 135, 137, 141
Diffusivity, 130, 131, 136, 137
Digital Versatile Disc (DVD), 40, 81, 84, 85, 89, 97, 100, 176, 194, 211, 220, 251, 252, 253–255, 256, 257, 258, 259, 271, 276, 285, 291
Digital Versatile Disc – Random Access Memory (DVD-RAM), 86, 209, 212, 219, 220, 252, 253, 255, 259, 272, 273, 279, 290
Digital Versatile Disc – Read Only Memory (DVD-ROM), 252, 253, 254, 255, 259
Digital Versatile Disc – Recordable (DVD±R), 253, 255
Digital Versatile Disc - ReWritable (DVD±RW), 81, 253, 255, 259, 279
Dihedral angle(s), 65, 66
Diode(s), 9, 10, 84, 91, 100, 220, 253, 260, 271, 280, 339, 383, 390, 391, 392, 401, 413, 414, 415
  based cell, 391
Dissipated power, 363, 364, 365
Distorted rock salt structure, 215
Distribution of data retention, 370
Dopants, 94, 96, 158, 219, 230, 243
Doping, 109, 159, 188, 230, 326, 357, 389
Driving motive force, 204, 205, 207
Drude dispersion model, 182, 183
Dual layer
  phase-change rewritable optical disc, 276
  recording, 270
DVD-RW (-RAM), 285
DVD, *see* Digital Versatile Disc (DVD)

E

E_A, 302, 304, 305, 322, 323
Early fails, 372, 373, 375, 376
e-beam, 342, 343
Edge contact, 332, 337, 338, 349
Effective medium approximation, 177
Elasticity power-law, 52
Elastic phase(s), 39, 52, 53, 54, 59
Electrochemical reaction, 233, 234, 236
Electrodeposition, 227, 233–238, 243, 244
Electrode(s), 6, 7, 9, 33, 104, 110, 115, 119, 187, 227, 231, 300, 301, 308, 309, 310, 311, 312, 313, 320, 332, 334, 337, 338, 341, 342, 343, 344, 349, 350, 377, 382, 385, 388, 393, 394, 395, 396, 397, 399, 400, 401, 402, 403
  materials, 233, 388, 395, 400
Electron
  beam lithography, 113, 115, 116, 242, 341
  diffraction, 67, 111, 157, 209
Electronegativity, 31
Electronic, 1, 2–3, 5, 17, 18, 19, 20, 21, 23, 24, 29–36, 71, 138, 144, 145, 149, 175, 184, 187, 189, 192, 195, 202, 219, 243, 251, 299, 306, 326, 409, 412
Electronic structure, 18, 24, 29, 33, 71, 326
Electronic switching, 187
Electroplating, 233
Electro-thermal, 364
  modeling, 309–313
Ellipsometry, 108, 175, 176, 177–178, 179
Endurance, 113, 232, 334, 343, 355, 356, 362, 363, 368, 377, 378, 381, 383, 393

Energy
barrier, 46, 317, 322, 323
dissipated, 363
Entropy, 30, 41, 42, 55, 58, 63, 144
Erasability, 92, 93, 266
Ergodic, 42, 48
Ernst Abbe, 286
Eutectics, 46
EXAFS, *see* Extended x–ray absorption fine structure (EXAFS)
Exchange-correlation
energy, 21, 22, 23
functional, 23
Extended x–ray absorption fine structure (EXAFS), 24, 25, 26, 27, 67, 68, 70, 71, 72, 73, 74, 75, 76, 152, 156, 157, 160, 163, 169, 215
Extinction coefficient (*k*), 108, 110, 220, 260

F

Feature, 3, 9, 10, 11, 42, 44, 52, 53, 78, 100, 152, 176, 178, 186, 192, 194, 199, 228, 238, 280, 292, 296, 301, 302, 308, 309, 311, 312, 331, 336, 342, 355, 357, 358, 360, 363, 388, 390, 391, 393, 402, 416
Femtosecond laser pulses, 118
Fermi-Dirac statistics, 192
Fermi level, 29, 30, 31, 32, 33, 34, 192, 193, 194, 295, 302, 303
Ferroelectric transition, 153
Field Effect Transistor (FET), 382, 383, 384, 390, 391, 398
based cell, 391
Film thickness, 100, 101–105, 106, 108–109, 114, 119, 139, 186, 221, 222, 227, 290, 293, 332, 337
Finite-differential time-domain (FDTD), 295
First sharp diffraction peak, 70
Flexible, intermediate and stressed-rigid, 39, 42, 59
Flexible-intermediate stressed-rigid classification, 57
Flexible phase, 52, 53, 54
Fluctuation electron microscopy, 67, 105
Footprint, 388, 391
Formation energy, 30, 235
Fragile, 39, 44, 57, 58, 131, 203
Fragile liquids, 57, 58, 131
Fragile and strong liquids, 44, 56, 57, 58, 131, 203
Free carrier absorption, 175, 181, 182
Free energies, 205

G

$Ge_2Sb_2Te_5$, 26, 27, 28, 29, 33, 40, 63, 69, 78, 84, 85, 86, 87, 102, 106, 113, 119, 138, 139, 140, 141, 143, 144, 145, 154, 155, 156, 157, 158, 160, 167, 169, 170, 175, 177, 178, 180, 181, 182, 183, 184, 185, 186, 187, 188, 189, 191–193, 194, 210, 211, 212, 213, 214, 215, 218, 219, 220, 221, 228, 229, 230, 231, 232, 241, 266, 286, 288, 290, 299, 334, 356, 358, 361, 387
bond lengths, 26, 70, 71, 73, 76, 78, 165, 169
coordination numbers, 28, 65, 67, 72, 73, 75, 165
EXAFS, 24, 25, 26, 27, 67, 68, 69, 70, 71, 72, 73, 74, 75, 76, 152, 156, 157, 160, 163, 169, 215
neutron diffraction, 25, 26, 68, 78, 153, 215
x-ray diffraction, 69, 70, 103, 106, 115, 151, 155, 156, 157, 158, 210, 214, 215, 229, 230, 235, 236, 239
General gradient approximation (GGA), 23
Germanates
anomaly, 54
$GeSb_2T_4$, 213
EXAFS, 70, 156
neutron diffraction, 70, 154, 156, 157
x-ray diffraction, 70, 155, 156, 157, 210
Ge-Sb, 63–79, 104, 106, 109, 149, 151, 152, 154–160, 170, 180, 182, 184, 191, 193, 210, 211, 212, 223, 263, 288, 334
Ge-Te, 28, 29, 31, 32, 65, 70, 71, 72, 74, 76, 78, 153, 164, 165, 168, 169, 208, 263
$GeTe-Bi_2Te_3$, 222, 223
$GeTe-Sb_2Te_3$, 85, 86, 118, 151, 154, 155, 157, 199, 209–213, 214, 215, 216, 217, 219, 220, 221, 222, 223, 263, 266
pseudo-binary system, 209–213, 223
Ge tetrahedral coordination, 73, 74, 77, 165
Gibbs-DiMarzio, 47

Gibbs model for crystal nucleation, 133
Glass
formation tendency, 45
forming tendency, 44–48, 51
transition, 39, 40, 41, 42, 43, 44, 45, 46–54, 56–57, 63, 82, 94, 132, 138–142, 143, 144, 150, 206, 265
nature of, 40, 42, 51
temperature, 39, 46–51, 56–57, 63, 82, 94, 132, 138–142, 143, 144, 150, 206, 265
Global phase diagrams, 53
Growth, 3, 30, 82, 86–89, 90, 94, 95, 96, 97, 99, 102, 104, 105, 106, 107, 110, 111, 112, 125, 135–137, 138, 139, 140, 141, 142, 144, 179, 182, 183, 187, 188, 206, 230, 233, 241, 251, 252, 263, 264, 266, 268, 269, 270, 279, 309, 315, 316, 317, 318, 334, 341, 342, 350, 355, 370, 374, 375, 389, 416
-dominated materials, 86, 87, 88, 105, 106, 110, 141, 144, 264, 269, 270, 279, 341, 350
GST, 64, 65, 67, 69, 76, 77, 102, 103, 104, 105, 108, 109, 111, 112, 113, 114, 115, 116, 118, 119, 228, 229, 230, 231, 232, 233, 242, 299, 300, 302, 306, 308, 309, 320, 334, 335, 336, 338, 340, 341, 344, 345, 356, 358, 359, 360, 361, 362, 363, 364, 365, 366, 367, 368, 369, 377, 387, 398, 399, 400, 401
thickness, 336, 363, 366, 367

H

Hall measurements, 189–190, 194
Heater, 190, 301, 311, 332, 333–336, 337, 338, 339, 349, 356, 358, 359, 360, 363, 364, 365, 366, 367, 377, 404
thickness, 363, 365, 366
Heterogeneous crystal nucleation, 133–135
Heteropolar bonds, 65
Heterostructures, 241
Hexagonal phase, 27, 28, 29, 102, 103, 109, 112, 114, 115, 116, 175, 177, 178, 180, 182, 183, 186, 187, 192, 193, 213, 214, 223, 229
High aspect-ratio nanowires, 237
High-K gate dielectrics, 40
High-performance applications, 361
High temperature superconductors, 40
High volume manufacturing, 356, 361
Hohenberg-Kohn theorem, 17, 19
Homogeneous crystal nucleation, 125–132, 143
Homogeneous electron gas, 22
Homologous series, 223
Homopolar bonds, 27, 28, 50, 65, 71, 74

I

Ideal glasses, 54–56
Incubation times, 100, 103, 104, 105, 106, 110, 113, 114, 141, 144, 145
for crystal nucleation, 144
Index of refraction, 176
Information storage, 1
Infrared reflectance, 42, 54
Initialization, 64, 277–279
Integrated circuit, 3, 9, 10, 228, 244, 410, 420, 427
Interfaces, 40, 87, 88, 89, 101, 102, 104, 106, 107, 109, 126, 129, 130, 133, 135, 136–137, 141, 176, 234, 242, 277, 279, 287, 317, 318, 319, 326, 334, 364, 365, 366, 367, 368, 377, 383, 394
Intermediate phase, 39, 42, 54
Intermediate-range order (IRO), 65
Isoconfigurational amorphous states, 132, 141
Isotropic scaling, 312, 313
Iterative write-verify scheme, 404

J

Jamming effect, 44
Johnson-Mehl-Avrami analysis, 138, 269
Joint density of states, 35
Joule heating, 187, 299, 300, 301, 306, 312, 383, 384, 388

K

Kauzmann temperature, 41, 44
Keyhole-transfer process, 402, 403
Kinetic specific heat, 48
Kissinger analysis, 138, 154
Kohn-Sham equations, 17, 20–22

L

Land/groove recording, 270, 271–272
Langevin dynamics, 25

Laser
ablation, 114, 116, 227
heating time for crystallization, 208, 211
LDA, *see* Local density approximation (LDA)
Lindemann's melting criterion, 47
Line Structure, 341–342
Liquid phase, 25, 26, 125, 205, 207, 218, 300, 309
Liquidus temperature, 46, 126, 142, 143
Lithographic size variability, 396, 397, 399, 403
Local density approximation (LDA), 17, 22–23, 68, 292, 294
Local order, 27, 28, 33, 36, 74, 75, 157, 160, 171, 178
parameter, 27, 28, 74, 75
LOCOS, 331
Lone pairs, 33, 194
Long-range structure, 66
Lorentz oscillator model, 177

M

Magnetic core memories, 3
Many-body perturbation theory, 24
Matchstick, 334
Material optimization, 93–97
Matrix elements, 31, 35, 36
Maxwell relation, 43
m-DSC, *see* Modulated-differential scanning calorimetry (m-DSC)
Mechanical constraints, 45
Medium-range order (MRO), 65–66
Melting, 9, 25, 26, 39, 42, 44, 47, 64, 82, 84, 99, 101, 111, 112, 114, 117, 118, 119, 126, 132, 136, 138, 142–145, 150, 153, 199, 201, 202, 204, 206, 239, 241, 242, 260, 261, 262, 263, 265, 268, 277, 289, 294, 300, 309, 310, 311, 312, 314, 319, 320, 331, 381, 384, 385, 386, 389
Melting point, 9, 26, 84, 101, 111, 112, 132, 150, 153, 201, 206, 242, 261, 262, 263, 265, 268, 294, 300, 309, 310, 314, 319, 320, 385
Melting temperature, 39, 82, 99, 111, 112, 114, 117, 126, 132, 136, 138, 142–145, 199, 202, 204, 241, 242, 262, 384, 386
Melt-quenching, 1, 64, 87, 111, 113, 118, 119, 144, 188, 206, 347, 356
vitrification, 64
Metal Oxide Semiconductor Field Effect Transistor (MOSFET), 3, 40, 356, 357, 361, 391
Metastable, 27, 28, 29, 41, 44, 63, 70, 71, 72, 74, 76, 79, 82, 103, 114, 132, 149, 150, 151, 154–157, 160, 171, 175, 177, 182, 186, 208, 213, 214, 215, 223, 229, 236, 266, 320, 322, 323
Metastable crystalline phase, 27, 28, 29, 154, 156, 160, 177, 215
Metastable cubic phases, 214, 223
Mobility, 48, 64, 82, 96, 150, 187, 189, 190, 191, 192, 193, 194, 206, 265, 269, 303, 307, 309, 317, 322
Metal-organic chemical vapor deposition (MOCVD), 228
Modulated-differential scanning calorimetry (m-DSC), 39, 42, 49, 57, 58
Molecular dynamics, 23, 24, 25, 26, 27, 68, 72, 78
Moore's law, 10, 99, 331
MOSFET, *see* Metal Oxide Semiconductor Field Effect Transistor (MOSFET)
Mössbauer mean square displacements, 47
Multilevel, 187–188, 260, 270, 275, 280, 281, 326, 350
Multilevel-cell, 344, 345
Multilevel data storage, 275
Multilevel operation, 270, 275, 280, 281, 326, 350
Multilevel PCRAM, 390, 403
Multilevel recording, 187–188, 260, 275, 280, 281
Mushroom, 232, 301, 334, 381, 382, 393–397, 398, 401
cell, 232, 301, 381, 382, 393–397, 398, 401

N

NA, 253, 256, 257, 259, 260, 270, 271, 275, 280, 286, 287, 291
Nanomaterials, 227, 241–243, 244
Nanoscale phase separation, 40, 47, 50, 52
Nanowire memory devices, 113
Near-field phase-change optical recording, 270
Negative coefficient of resistance, 1
Negative differential resistance, 187, 306, 307

Neutron
diffraction, 25, 26, 68, 78, 153, 215
scattering, 26, 70
-scattering lengths, 70
N/G, 309, 314, 315, 316, 317, 319, 320
NMR, *see* Nuclear magnetic resonance (NMR)
Non-ergodic, 42, 48
Non-reversing enthalpies, 39, 57, 58
Non-reversing heat flow, 49, 50
Non-thermal melting, 118, 119
Non-volatile memory, 355, 362, 369, 378, 406
8-*N* rule, 72, 77, 79
Nuclear magnetic resonance (NMR), 67
Nucleation, 82, 86–88, 89, 94, 95, 96, 102, 104, 105, 106, 107, 110, 125, 126, 127, 128, 129–132, 133–135, 136, 137, 138, 139, 140, 141, 142, 143, 144, 151, 179, 187, 205, 206, 207, 209, 230, 233, 242, 263, 264, 266, 269, 270, 279, 309, 315, 316, 317, 318, 320, 334, 341, 342, 370, 374, 375, 389
-dominated materials, 86, 87, 105, 106, 141, 144, 264, 269, 270, 279, 334, 341, 342, 389
probability, 87, 88, 96, 233

O

Octahedral
-like geometry, 74
local geometry, 26, 76
Optical, 7, 10, 13, 24, 32–35, 52, 54, 64, 81–85, 92, 94, 96, 100–108, 118, 144, 149, 151, 154, 162
Optical constants, 96–97, 108, 154, 176–185, 202, 211, 265
Optical contrast, 32, 34, 36, 84, 94, 97, 178–179, 211, 219–220, 266
Optical discs, 13, 83–84, 105, 109, 119, 167, 202, 212, 214, 221–223, 252, 259–262, 264, 267–268, 272, 274–281
Optical elasticity, 52, 54
Optical memory, 13, 100, 154, 199–200, 202, 206, 209, 251–281, 285
Optical recording, 81, 84, 92, 94, 96, 154, 257, 259, 260, 262–263, 266, 270, 274, 275, 280
technology, 259
Overwriting, 212, 252, 262, 263, 277
Ovonyx, 11–13

P

Pair correlation function, 23, 25, 26, 69, 70
Partial pair distribution functions, 72, 73
Partial-Response Maximum Likelihood, 273
Peierls transition, 26
Percolation
path, 370, 375
Phase
separation, 50, 52, 136, 205–207, 264–266
transformation, 175–180, 184, 186–188, 244, 314–320, 325, 388
δ - Phase, 223
Phase change
materials, 1, 7, 9–11, 18, 24, 25, 28, 29, 33, 36, 40–41, 51, 69, 81, 84–87, 89–97, 99–119, 129, 132, 136, 137, 138, 142–143, 149–170, 175–177, 184, 187–189, 199–207, 210, 215–218, 221–222, 227–233, 235, 237–243, 260–269, 276, 285
memory, *see* Phase Change Memory (PCM)
nanocrystals, 105, 242
nanoparticles, 114–118
nanowires, 111–114
optical discs, 202, 214, 260–268, 275–279
optical storage, 260, 264–267, 270, 279
random access memory, 13, 40, 81, 99, 118, 228, 331–349, 381–405
Phase Change Memory (PCM)
array, 9, 383
cell, 9, 355–378, 381, 382, 386
device, 326, 376, 377
modeling, 326
scaling, 313
storage element, 356, 357, 363, 364
See also Scaling
Phase change random access memory (PCRAM), 40, 81, 100, 102, 104, 105, 106, 109–111, 113–114, 118–120, 186–188, 194, 228, 230–232, 235, 238, 240, 243, 296, 331, 342, 347, 350, 381, 387–392, 403
Photoconductivity, 184, 185, 321

Photodarkening, 185
Photoemission spectroscopy, 24, 71, 193
Photo-induced current, 184–185
Photo-oxidation, 185
Pillar
  cell, 340, 393, 397–399
  structure, 340–341
Plasma enhanced chemical vapor deposition (PECVD), 228, 341
Plasmons, 287–292
Polyalcohols, 57
Poole-Frenkel (PF), 302, 303, 306–307, 309, 321–323, 349
Pore cell, 393, 397, 399–400
Potential energy landscape, 44
Potential deposition, under, 235
Power dissipated, 343, 365
Precursors, 227–233, 238–241
Primed phase, 105
Process
  integration, 336, 379, 406
  variation, 336, 339, 386
Programming
  cell, 385
  current, 300, 310, 312, 313, 320, 332, 357–368, 386, 390, 395
  techniques, 403
  variability, 404
Protein folding, 40
Pseudobinary line, 27, 266
PVD GST deposition, 400

R

Radial distribution function, 65
Raman
  pressure experiments, 55
  scattering, 39, 42, 52, 54, 153
Random access memory, 3, 13, 40, 99, 118, 186, 199, 209, 228, 252, 331–349, 381–405, 413
Random-phase approximation, 34
Reactive ion etching (RIE), 228, 341, 394, 396–400, 403
  of the GST, 399
Read, 9, 84, 109, 252–259, 263–268, 274, 276, 286, 308, 310–312, 325, 345, 355, 357, 361, 373, 378, 382–390
Read operation, 313, 373
Reflection, 82, 89, 90–92, 96–97, 176–177, 185, 254, 257, 268, 275, 281, 348, 349
Refractive index, 108, 110, 200, 220, 260, 268, 276, 286–289, 293, 295
Relaxation activation energy, 142
RESET
  current, 112–113, 188, 191, 228, 238, 240, 243, 310, 335–340, 343–350, 378, 385, 389–393, 395, 397–400
  operation, 9, 10, 111, 119, 300, 301, 309, 310, 362, 363, 373, 375, 376, 384, 396
  pulse widths, 362, 363
Resistance distributions, 370, 373, 403, 405, 386, 393
Resistivity, 1, 5, 101, 102, 103, 104, 105, 108, 109, 149, 186–187, 188, 194, 230, 240, 300, 301, 334, 343, 356, 357, 362, 367, 390, 395
Retention
  loss, 369, 370, 372, 374
  specification, 390
Reverse-Monte Carlo (RMC), 68–78, 215, 218
  simulation, 68, 72, 78, 215
Reversibility windows, 42, 54, 55
Reversing heat flow, 49, 50, 58
Re-writable DVDs or CDs, 40
Rewritable optical recording, 81, 96
Rigid but stressed phase, 52
Ring
  electrode, 393–397
  structures, 27, 218, 332, 338–339, 349
Ring-size
  analysis, 74
  distribution, 74, 75
Rocksalt
  structure, 32, 72, 74, 76, 152–159, 165–168, 214, 216

S

Sb_2Te, 94–95, 103, 115–116, 138, 140, 141, 144, 158, 170, 219, 242, 292
Scalability, 100, 101, 111, 242, 343, 355, 379, 382
Scaling
  PCM, 326
  properties, 99–119
Scanning probe microscopy, 231
Scattering wave vector transfer, 67
Seebeck coefficient, 190, 194
Selecting device, 356, 357
Self-Aligned μTrench, 358

Self-assembly based lithography, 116
Self-organized, 40
SET, 118, 119, 331, 337, 343, 345, 347, 348, 384, 385, 386, 387, 388, 389, 393, 394, 395
resistance, 313, 357, 363, 368, 386, 387, 395
Set operation, 5, 9, 10, 300, 314, 363, 384
Set pulse widths, 384
Shear viscosity, 130, 131, 142
Short-range order, 64–65, 160, 164, 165, 167
Simple cubic, 209, 210, 215, 216, 218
structure, 209, 210, 215
Single phase, 151, 188, 199, 205, 210, 221
Soluble precursor, 238
Solution-phase deposition, 238, 243
Spinel, 33
Square-like rings, 75, 76
Static
RAM, 3
tester, 92
Stochastic agglomeration theory, 46, 51
Stoichiometric compounds, 158, 207, 208, 214
Stokes-Einstein equation, 130, 131, 142
Stretched exponents, 53, 57
Strong-fragile classification, 57
Strong liquids, 56, 57
Structural design, 382
Structural modeling, 68
Structural relaxation, 31, 51, 132, 142, 299, 320, 321
of amorphous phase, 320
Structure factor, 23, 25, 27, 67, 70, 74
Sub-lithographic features, 358
Supercell, 29, 30
Superlattice-like structure, 109
Super-RENS, 285–296
Super resolution
near-field structure, 260, 285–296
Switching speed, 100, 118–120, 149, 151, 189, 286, 306, 342

T

Tauc relationship, 179, 180
Te-based eutectic compositions, 203, 204
Te-based single phase materials, 206
Te-Ge, 28, 73, 168, 203
$Te_{85}Ge_{15}$, 208, 219
$Te_{80}Ge_5Sn_{15}$, 208, 209, 210
$(Te_{80}Ge_5Sn_{15})_{100-x}Au_x$, 208, 209
TeGeSnAu, 215, 216
Temperature
dependence, 129, 180, 186, 191, 193, 217, 302, 319, 320, 322, 325
factor, 154, 216, 217
Terminal atoms, 45
Te-Sb, 168, 203, 292, 294
Thermal conductivity, 109, 184
Thermal stability, 101, 109, 205, 207, 262, 265
Thermal vibration, 130, 216–218
Thermodynamic specific heat difference, 50
Thermoelectric effect, 190–191
Thomson effect, 191, 343
Threshold switching, 10, 13, 109, 113, 115, 151, 301, 302, 306, 307, 383
Time dependent density functional theory, 24, 34
Transmission, 2, 82, 96, 105, 138, 152, 164, 176, 177, 182, 185, 230, 231, 265, 276, 360, 427, 385, 413
Transmission Electron Microscopy (TEM), 2, 82, 105, 138, 152, 230
Transport properties, 24, 30, 33, 189, 194
μTrench, 332, 338, 349, 381, 393, 399
cell, 308, 357, 359, 381, 393, 399
optimized structure, 367
Trimming, 228, 340, 342, 397
Turnbull-Fisher model for crystal nucleation, 129

U

Ultraviolet photoemission spectroscopy (UPS), 24, 71
Undercooled liquid, 129, 131, 132, 138, 142
phase change materials, droplets of, 142
Urbach edge, 181–182, 183, 194
UV light, 280

V

Vacancies, 27, 29, 30, 31, 70, 74, 75, 76, 155, 156, 157, 164, 181, 191, 192, 193, 213–215, 308, 322

Valence
alternation pairs, 33
-band density of states, 71
Vapor-phase amorphous-film deposition, 64
Variability, 337, 371, 372, 378, 381, 386, 387, 388, 396, 397, 398, 399, 401, 402, 403, 404, 406
Via filling, 231, 235
Vibrational entropy, 58
Viscosity, 25, 43, 44, 46, 56, 57, 63, 69, 96, 130, 131, 132, 136, 141, 142, 202, 240, 265
Volmer's spherical cap model for heterogeneous crystal nucleation, 133
Volmer-Weber model for crystal nucleation, 128
Voltammetry, 233
Volume-minimized, 397, 399

W

Window glass, 40

X

X-ray
absorption near-edge structure, *see* X-ray absorption near-edge structure (XANES)
absorption spectroscopy, 67
diffraction, *see* X-ray diffraction (XRD)
photoemission spectroscopy, *see* X-ray photoemission spectroscopy (XPS)
scattering factors, 70
X-ray absorption near-edge structure (XANES), 67, 163, 164, 165, 167, 168, 169
X-ray diffraction (XRD), 69, 70, 72, 73, 74, 75, 103, 106, 115, 116, 117, 151, 155, 156, 157, 158, 210, 214, 215, 229, 230, 235, 236, 239, 275
See also $Ge_2Sb_2Te_5$;$GeSb_2T_4$
X-ray photoemission spectroscopy (XPS), 24, 71, 72, 193

Z

Zeldovich factor, 129